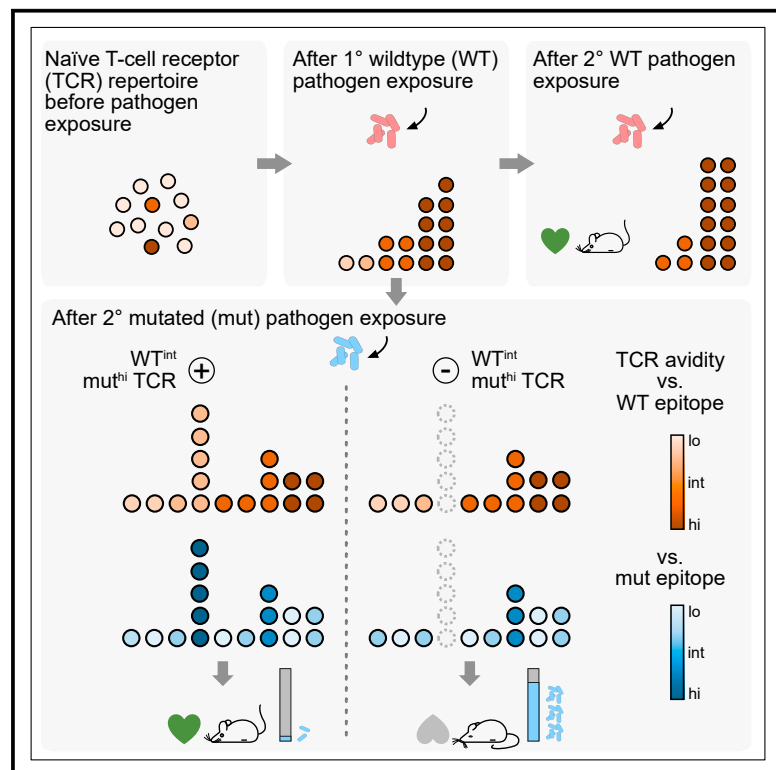


# Immunity

## Recruitment of epitope-specific T cell clones with a low-avidity threshold supports efficacy against mutational escape upon re-infection

### Graphical abstract



### Authors

Adrian Straub, Simon Grassmann,  
Sebastian Jarosch, ...,  
Veit R. Buchholz, Kilian Schober,  
Dirk H. Busch

### Correspondence

kilian.schober@uk-erlangen.de (K.S.),  
dirk.busch@tum.de (D.H.B.)

### In brief

High-avidity CD8<sup>+</sup> T cells provide protective immunity. However, their recruitment into immune responses alongside lower avidity T cells is not well understood. Straub et al. here show that rare high-avidity clones are selectively expanded from naive precursor repertoires with heterogeneous functionalities. Such polyclonal recruitment enables flexible immune responses against heterologous re-infection.

### Highlights

- TCR avidity distribution in naïve donors is highly skewed
- Clonal T cell expansion upon infection is governed by clear TCR avidity thresholds
- The cross-reactivity landscape of single TCRs correlates with functional avidity
- Recruitment of broad TCR repertoires enables flexible immune responses



## Article

# Recruitment of epitope-specific T cell clones with a low-avidity threshold supports efficacy against mutational escape upon re-infection

Adrian Straub,<sup>1</sup> Simon Grassmann,<sup>1,2</sup> Sebastian Jarosch,<sup>1</sup> Lena Richter,<sup>1</sup> Philipp Hilgendorf,<sup>1,3</sup> Monika Hammel,<sup>1</sup> Karolin I. Wagner,<sup>1</sup> Veit R. Buchholz,<sup>1</sup> Kilian Schober,<sup>1,3,4,6,\*</sup> and Dirk H. Busch<sup>1,5,6,7,\*</sup>

<sup>1</sup>Institute for Medical Microbiology, Immunology and Hygiene, Technische Universität München (TUM), Munich, Germany

<sup>2</sup>The Joseph Sun Lab, Memorial Sloan Kettering Cancer Center, New York, NY, USA

<sup>3</sup>Mikrobiologisches Institut – Klinische Mikrobiologie, Immunologie und Hygiene, Universitätsklinikum Erlangen, Friedrich-Alexander-Universität (FAU) Erlangen-Nürnberg, Erlangen, Germany

<sup>4</sup>Medical Immunology Campus Erlangen, Friedrich-Alexander-Universität (FAU) Erlangen-Nürnberg, Schlossplatz 1, 91054 Erlangen, Germany

<sup>5</sup>Partner site Munich, German Center for Infection Research (DZIF), Munich, Germany

<sup>6</sup>These authors contributed equally

<sup>7</sup>Lead contact

\*Correspondence: [kilian.schober@uk-erlangen.de](mailto:kilian.schober@uk-erlangen.de) (K.S.), [dirk.busch@tum.de](mailto:dirk.busch@tum.de) (D.H.B.)

<https://doi.org/10.1016/j.immuni.2023.04.010>

## SUMMARY

Repetitive pathogen exposure leads to the dominant outgrowth of T cell clones with high T cell receptor (TCR) affinity to the relevant pathogen-associated antigens. However, low-affinity clones are also known to expand and form immunological memory. While these low-affinity clones contribute less immunity to the original pathogen, their role in protection against pathogens harboring immune escape mutations remains unclear. Based on identification of the TCR repertoire and functionality landscape of naive epitope-specific CD8<sup>+</sup> T cells, we reconstructed defined repertoires that could be followed as polyclonal populations during immune responses *in vivo*. We found that selective clonal expansion is governed by clear TCR avidity thresholds. Simultaneously, initial recruitment of broad TCR repertoires provided a polyclonal niche from which flexible secondary responses to mutant epitopes could be recalled. Elucidating how T cell responses develop “from scratch” is informative for the development of enhanced immunotherapies and vaccines.

## INTRODUCTION

Antigen-specific adaptive immune responses arise from a polyclonal repertoire of naive precursor populations.<sup>1,2</sup> Before antigen encounter, 1 in 10<sup>4</sup>–10<sup>6</sup> CD8<sup>+</sup> T cells are thought to recognize an individual epitope, presented by major histocompatibility complex (MHC) class I glycoproteins.<sup>3–7</sup> In an entire mouse organism, this corresponds to a few hundred CD8<sup>+</sup> T cells.<sup>6</sup> In terms of their T cell receptor (TCR) repertoire, naive T cell precursor populations are thought to be highly diverse,<sup>8</sup> largely consisting of unique clonotypes spanning a wide distribution of TCR avidities.<sup>9,10</sup>

Upon antigen encounter, individual T cell clones from this precursor population are recruited into the immune response, clonally expand, and differentiate into effector and memory subsets.<sup>11,12</sup> Within this evolutionary process of adaptation to an antigen, T cells harboring a high-avidity TCR are preferentially selected during the acute phase of an immune response<sup>13,14</sup> in a highly reliable manner.<sup>15</sup> However, depending on the epitope and type of immune response, antigen-experienced effector and memory T cell populations maintain TCR repertoires of

different diversity and avidity distributions following clonal selection and expansion.<sup>8,16–22</sup> Notably, chronic antigen exposure can lead to reversed hierarchies of TCR repertoires, with intermediate- or even low-avidity T cells increasingly dominating, e.g., during latent cytomegalovirus (CMV) infection.<sup>23</sup> Generally, low-avidity T cells have been shown to be of functional importance in various settings.<sup>24</sup>

Despite this extensive body of knowledge, several fundamental questions surrounding the evolution of antigen-specific T cell responses have barely been addressed. Specifically, it is unclear (1) which kind of avidity distribution is present in naive antigen-specific precursor populations, (2) which fraction of -precursor clonotypes are recruited and expand, (3) which TCR avidity thresholds govern these two processes, and (4) what the role is of low-avidity T cells that were initially recruited and only weakly expanded during primary immune responses. A central reason for this is the methodological difficulty to follow a polyclonal TCR repertoire, for which the avidities of individual constituents are known, from its beginning as a naive precursor population throughout activation and expansion during an immune response.



Here, we identified, characterized, and synthetically rebuilt representative antigen-experienced and naive TCR repertoires directed against the H2K<sup>b</sup>-restricted ovalbumin (OVA) model epitope OVA<sub>257–264</sub> (SIINFEKL). We analyzed repertoires via a combination of single-cell RNA sequencing (scRNA-seq) and TCR sequencing, flow cytometry-based “speed enrichment,” and transgenic TCR re-expression in color-coded retrogenic mice. TCR characterization was based on in-depth *in vitro* and *in vivo* functionality assays, including transfer experiments with defined polyclonal populations entailing 10 different, barcoded TCRs. Analyzing 52,804 purified antigen-reactive T cells from 40 mice after antigen encounter, as well as naive precursor populations from 18 mice, allowed extensive investigation of TCR repertoires. We assessed the functionality landscape of antigen-specific naive precursor populations and identified distinct avidity thresholds for clonotypic recruitment and expansion upon bacterial infection with *Listeria monocytogenes* (Lm). Systematic cross-reactivity mapping of 5,016 unique TCR-peptide (p)MHC interactions revealed that functionality toward the cognate epitope SIINFEKL largely correlated with reactivity toward mutant epitopes. However, we also identified several individual clonotypes that are of low avidity against the wild-type (WT) epitope, but of high avidity against mutant epitopes. Such clonotypes did not strongly expand after immunization with the WT epitope but dominated heterologous recall responses and were then also critical for protection. These findings demonstrate that clonal expansion and polyclonal recruitment of TCR repertoires with a low avidity threshold jointly ensure tailored but flexible immune responses.

## RESULTS

### Primary CD8<sup>+</sup> T cell responses are highly polyclonal but dominated by a small number of high-avidity clonotypes

We first set out to investigate how many different T cell clonotypes are present and dominant in endogenous antigen-reactive T cell responses. To this end, we analyzed the endogenous CD8<sup>+</sup> TCR repertoire of 40 WT C57BL/6 mice after infection with recombinant Lm expressing the SIINFEKL peptide (Lm-SIINFEKL) of chicken OVA. We isolated SIINFEKL-reactive CD8<sup>+</sup> T cells via fluorescence-activated cell sorting (FACS) in two different manners (Figures 1A and S1A). On the one hand, we sorted H2K<sup>b</sup>/SIINFEKL-multimer-binding CD8<sup>+</sup> T cells. However, pMHC multimer binding may not capture all antigen-reactive T cells, particularly low-avidity clonotypes, and reversely has also been described to result in false-positive unspecific binding.<sup>25</sup> Therefore, we also isolated CD44<sup>hi</sup> CD8<sup>+</sup> T cells and defined antigen reactivity by the response to antigenic peptide after short-term co-incubation *ex vivo*, which we detected through transcriptomic shifts after scRNA-seq and TCR sequencing (“reverse phenotyping”<sup>26</sup>).

Uniform manifold approximation and projection (UMAP<sup>27</sup>) and Leiden clustering<sup>28</sup> of T cells sorted for CD44 expression identified a group of cells (Leiden cluster 3; Figure 1A) that showed a high T cell activation score (Figure 1B) and was particularly prominent after antigen-specific stimulation (Figures 1C and S1B). TCR clonotypes in the same cluster 3 were clonally expanded (Figure 1A), suggesting that these clusters could contain responding T cells to infection. Leiden cluster 3 was

characterized by expression of genes associated with activated and cytokine releasing T cells such as *Ifng*, *Tnfrsf9*, *Xcl1*, and *Cc14* (Figure 1B). We could therefore identify SIINFEKL-reactive clonotypes within CD44<sup>hi</sup>-sorted T cells based on the expression of these genes. In addition, TCR clonotypes derived from H-2K<sup>b</sup>/SIINFEKL-multimer<sup>+</sup>-sorted cells were identified. Upon antigenic stimulation, pMHC multimer<sup>+</sup> CD8 T cells were also recruited to Leiden cluster 3, validating our approach to define antigen-reactive T cells through transcriptomic shifts (Figure S1B).

Identification of antigen-reactive T cells allowed us to analyze the diversity distribution of clonotypes by calculating the Gini skewing index.<sup>29</sup> We identified a narrowing of the TCR repertoire in SIINFEKL-reactive clonotypes (activation score positive, A+, or multimer positive, M+), compared with less expanded unidentified specificities in activation score-negative (A-) or multimer-negative (M-) T cells (Figure 1D). This reduced TCR repertoire diversity is explained by a loss in evenness through clonal expansion. However, the overall antigen-reactive repertoire remained highly diverse in terms of richness of TCR sequences (Figure S1C). Furthermore, the identified TCR clonotypes neither clustered specifically according to clonal expansion nor to isolated donor or isolation method (activation score or multimer) (Figure S1C). Overall, we detected more than 1,000 unique SIINFEKL-reactive clonotypes in 40 mice (Table S1). Per mouse, we identified a median population size of 23 (A+) to 39 (M+) unique SIINFEKL-reactive clonotypes (Figure 1E). Irrespective of how antigen-reactive T cells were identified (activation score or multimer), 2–3 clonotypes per mouse dominated the immune response through clonal expansion (Figure 1F).

In summary, antigen-reactive T cell responses are highly polyclonal but simultaneously very skewed in terms of clonal distribution, suggesting clonal expansion of few high-avidity clonotypes per individual.

### Speed enrichment enables access to naive antigen-specific precursor populations that show an almost perfectly even distribution of TCR clonotypes

The analysis of clonally expanded SIINFEKL-reactive T cells that are recruited into a primary immune response most likely only represents the tip of the iceberg in terms of amount and diversity of the clonotypes that can be reactive to the antigen. To capture “whole” repertoires of antigen-specific precursor populations, we isolated single naive CD8<sup>+</sup> SIINFEKL-reactive T cells from antigen-unexperienced C57BL/6 donor mice (Figure 2A; Table S2). We utilized a sensitive FACS-based cell enrichment (speed enrichment; Figure 2B) to access antigen-reactive T cells from extremely small precursor populations. Specificity following sorting was confirmed by two different H-2K<sup>b</sup>/SIINFEKL multimers, including spiked-in OT-I cells as reference (Figures 2B and S2A). Sorted single-cell clones expressed CD62L and low amounts of CD44, as expected for naive T cells (Figure 2B), and were expanded in an antigen-unspecific manner (by anti-CD3, anti-CD28, and IL-2) *ex vivo*.<sup>30</sup> We observed variable precursor population sizes of naive SIINFEKL-reactive CD8<sup>+</sup> T cells between donors, which were on average (mean = 149.7) comparable to previously reported numbers (120–170).<sup>6</sup> Of note, upon correcting our data to the recovery of OT-I control cells to account for yield loss during cell enrichment, we detected less variable and generally larger (mean = 350.9)

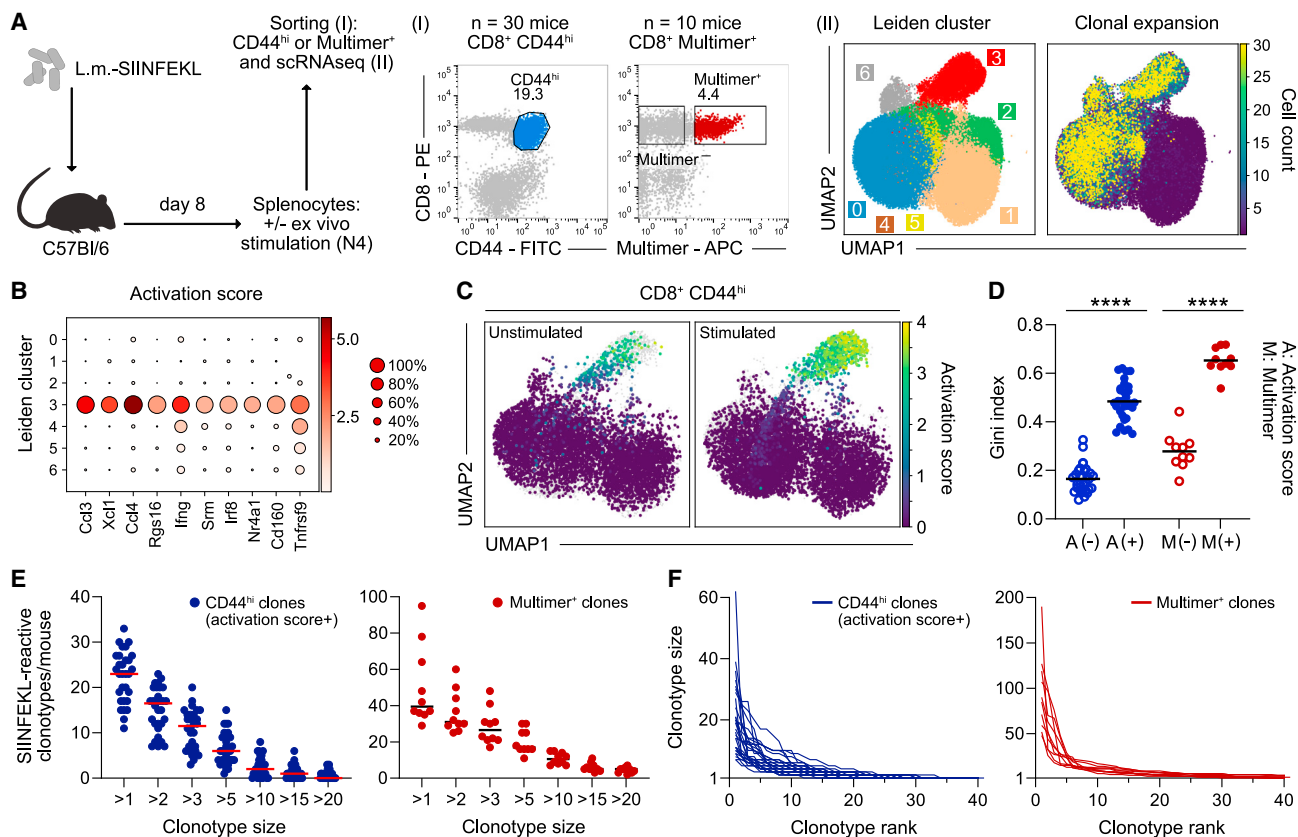


**Figure 1. Primary CD8<sup>+</sup> T cell responses are highly polyclonal but dominated by a small number of high-avidity clonotypes**

(A) Schematic: 40 WT C57BL/6 mice were infected with *Listeria monocytogenes* (Lm)-SIINFEKL. At day 8 p.i., splenocytes were collected from each recipient and stimulated with SIINFEKL peptide or left untreated. (I) 3,000 CD8<sup>+</sup> T cells were sorted for CD44<sup>hi</sup> (n = 30 mice) or for H-2K<sup>b</sup>/SIINFEKL multimer (n = 10 mice) and profiled by single-cell RNA sequencing (scRNA-seq). (II) Uniform manifold approximation and projection (UMAP) of Leiden clusters (left panel) and clonotype expansion (right panel) of combined experiments.

(B) Dot plot of log-normalized expression (color) and frequency (size) of selected marker genes across Leiden clusters (activation score).

(C) Activation score of unstimulated (left panel) and stimulated (right panel) cells.

(D) Gini index to assess TCR skewing based on the CDR3 pairs of activation score-negative (empty, blue circles), activation score-positive (filled, blue), multimer-negative (empty, red circles), and multimer-positive (filled, red) clonotypes. Higher Gini index indicates less diversity in CDR3 sequences.

(E) Amount of SIINFEKL-reactive-defined clonotypes in each mouse based on activation score (blue, left) or multimer staining (red, right), grouped by clonotype size.

(F) Clonal expansion of SIINFEKL-reactive-defined clonotypes in each mouse based on activation score (blue, left) or multimer staining (red, right), sorted by clone size. Sort data in (A) are representative of 30 (CD44<sup>hi</sup>) and 10 (multimer<sup>+</sup>) mice. scRNA-seq data (All) are 40 mice pooled from four independent experiments. Data in (B), (D), (E), and (F) are pooled from four independent experiments. Data in (C) are representative of three independent experiments. Each dot in (D) and (E) and each line in (F) represent the repertoire of one mouse; lines indicate mean. Statistical testing was done using a two-sided Mann-Whitney test. \*\*\*p < 0.0001. See also Figure S1.

population sizes, relating to 1 in every 33,000 CD8<sup>+</sup> T cells per donor (Figure 2C).

We further analyzed the TCR repertoire after single-cell PCR and TCR sequencing of isolated clones and found an almost perfectly even distribution of CDR3 sequence diversity over 9 naive mouse repertoires. We observed 4 repetitive CDR3 $\beta$  sequences with differential CDR3 $\alpha$  pairing, 4 repetitive CDR3 $\alpha$  with differential CDR3 $\beta$  pairing, as well as two duplicate  $\alpha\beta$  clones found in the same host, which likely underwent homeostatic proliferation (Figure S2B; Table S2). Given the conserved repertoire size and frequency, but large diversity in clonotypes, we chose the SIINFEKL-reactive repertoire of a single C57BL/6 donor to further investigate and “re-build” a representative naive repertoire. We re-expressed 18 identified full  $\alpha\beta$  TCRs in retro-

genic mice<sup>31,32</sup> as a source for TCR transgenic naive CD8<sup>+</sup> T cells (Figures 2E and 2F; Table S2). To allow tracking of our transgenic populations, we utilized congenic strains expressing combinations of CD45.1/CD45.2 and/or CD90.1/CD90.2, as well as combinatorial transductions with different retroviruses, encoding for the fluorescent proteins GFP, YFP, Ametrine, CFP, and BFP (GYACB; Figures 2E and S2C), as previously demonstrated.<sup>32,33</sup> All TCR transgenic T cell populations retained a positive H2K<sup>b</sup>/SIINFEKL multimer staining, although staining intensities were highly variable between clonotypes and included poor binders, indicating a diverse distribution in TCR avidities (Figure 2F).

In summary, naive antigen-reactive precursor populations are larger than previously estimated and highly diverse in terms of

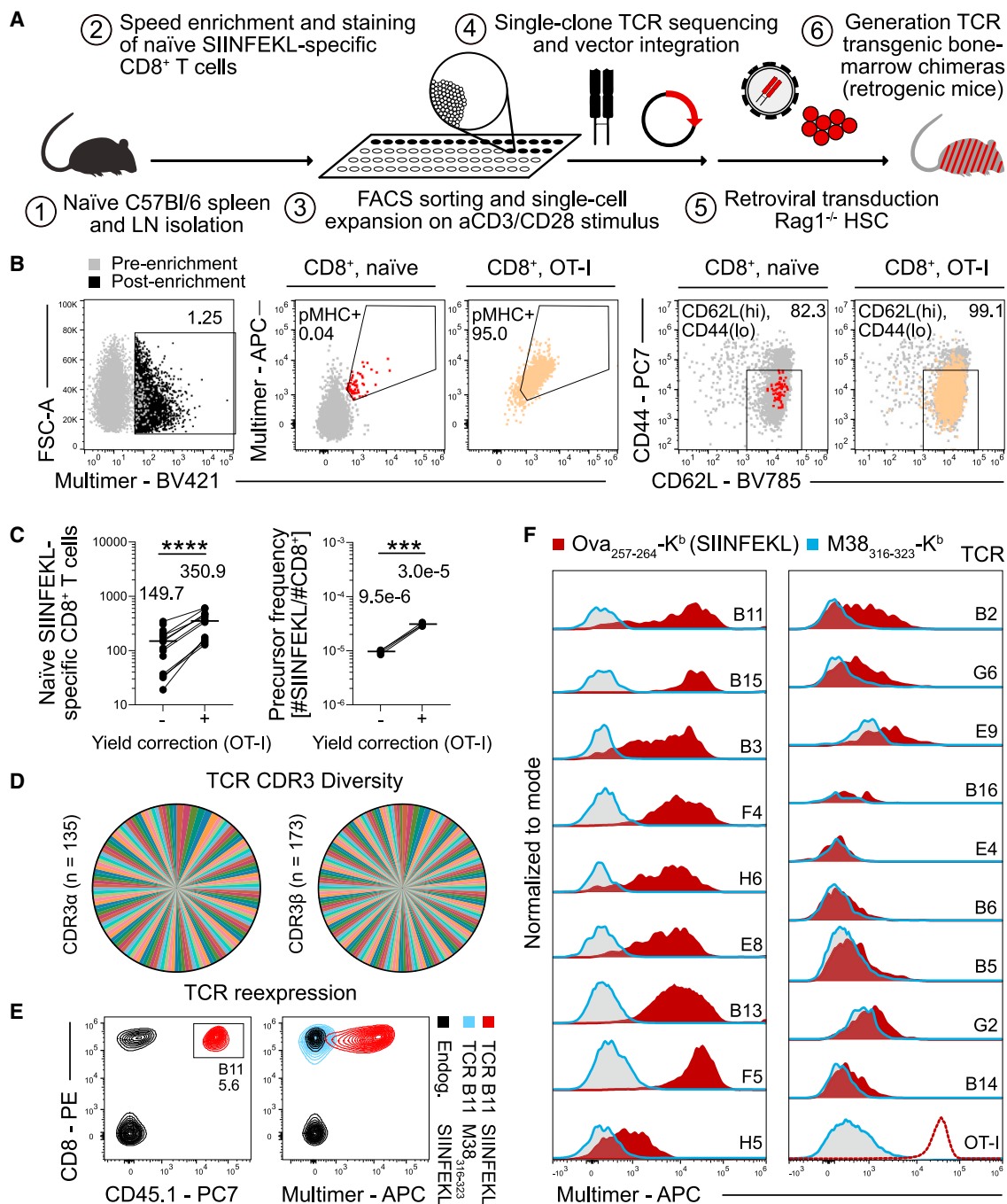


**Figure 2. Speed enrichment enabled access to naïve antigen-specific precursor populations that show an almost perfectly even distribution of TCR clonotypes**

(A) Schematic: spleen and lymph node preparation of naïve C57BL/6 mice followed by speed enrichment and double multimer staining (H-2K<sup>b</sup>/SIINFEKL) to isolate SIINFEKL-reactive naïve CD8<sup>+</sup> T cells. TCR sequences were isolated from expanded single cells and cloned into a retroviral vector. Rag1<sup>-/-</sup> HSCs were transduced with TCR retrovirus and transferred into irradiated C57BL/6 recipients to generate retrogenic mice.

(B) Left to right: dot plots depict speed enrichment on H2K<sup>b</sup>/SIINFEKL multimer, double multimer staining of SIINFEKL-reactive CD8<sup>+</sup> T cells and of spiked-in OT-I cells, as well as respective phenotypes based on CD44 and CD62L, representative of 18 independent experiments.

(C) Scatterplots depict counts (n = 18) and frequencies (n = 4) of naïve SIINFEKL-reactive CD8<sup>+</sup> T cells per mouse. Yield correction is based on recovery of spiked-in OT-I cells after speed enrichment.

(D) Clonotype diversity of CDR3 $\alpha$  and CDR3 $\beta$  sequences from 9 C57BL/6 mouse repertoires.

(legend continued on next page)

clonal distribution. Barcoded transgenic re-expression of identified TCRs from a single mouse provided us with a toolbox to further investigate and re-build a defined polyclonal repertoire that is representative for naive precursor populations.

### TCR avidity distribution of antigen-specific precursor populations in naive donors is highly skewed

The clonal dominance of few clonotypes per mouse in antigen-reactive T cell populations (Figures 1E and 1F) suggested that only a minor fraction of TCRs present in the precursor repertoire recognize the antigen with high avidity. To test this intuitive but experimentally barely addressed hypothesis, we assessed TCR functional avidity (antigen sensitivity) after antigen-specific stimulation, as well as TCR structural avidity by  $k_{off}$ -rate measurements.<sup>34</sup> We found two TCR clonotypes, TCRs B11 and B15, with structural avidities displaying a mean  $k_{off}$  rate of 64.0 and 36.2 s, respectively (Figures 3A and S3A). The TCR-pMHC binding strength of the remaining TCRs was below the detection limit of this assay. Stimulation with SIINFEKL peptide confirmed a high functional avidity for B11 and B15 (Figure 3B). TCRs B11 and B15 downregulated the CD3-TCR complex at low peptide concentrations relating to EC<sub>50</sub> values of 10<sup>-10.4</sup> and 10<sup>-9.7</sup> M, respectively. In line, all cells of both clonotypes upregulated CD69 after 18 h of stimulation at a peptide concentration of 10<sup>-10</sup> M (Figures 3C, 3D, and S3B). Some TCRs without a measurable  $k_{off}$  rate, such as TCR B3, still displayed strong CD3 downregulation and CD69 upregulation after stimulation. Such TCRs were classified as “intermediate-avidity TCRs.” Other clones, such as TCR H6, barely showed CD3 downregulation but clearly showed upregulated CD69 upon stimulation with high peptide concentrations (“low-avidity TCRs”). Finally, another group of TCRs did not downregulate CD3 and barely or never upregulated CD69, even after stimulation with high peptide concentrations (“unreactive TCRs”). Notably, we observed only a mild correlation between multimer staining intensities of TCRs and functional avidity (Figure S3C).

In general, we identified downregulation of the TCR-CD3 complex after antigenic stimulation to be a sensitive marker to discriminate functional avidities between naive CD8<sup>+</sup> T cells (Figure 3C). To validate our results and enable large-scale comparisons of different TCRs, we introduced our TCR library into a human Jurkat triple parameter reporter (JTPR) cell line.<sup>35</sup> We assessed antigen sensitivity by peptide stimulation (Figures 3E and 3F) and found a significant correlation ( $R^2 = 0.93$ ) between expression of the nuclear factor of activated T cells (NFAT) transcription factor in JTPR and downregulation of the TCR-CD3 complex in primary murine T cells (Figure 3G). In all screenings (primary murine T cells and JTPRs), we observed the TCRs E4, G2, B16, and B14 to be non-responsive to SIINFEKL antigen, although they were isolated based on SIINFEKL multimers and

showed restaining after non-specific expansion *ex vivo* (Figure S3D). This phenomenon has been previously described and may stem from non-agonist TCR-pMHC interactions.<sup>36</sup> Of note, these TCRs also showed weak multimer binding after re-expression (Figure 2F). This highlights the value of transgenic TCR re-expression for validation and interrogation of TCR functionality.

To contextualize these TCR functionalities derived from the naive repertoire, we assessed antigen sensitivity in the same manner for “antigen-experienced” TCRs derived from mCMV-IE2-SIINFEKL-infected C57BL/6 recipients,<sup>23,37</sup> which showed consistently high functionalities (Figures 3E and 3F). From the naive repertoire, only the identified high-avidity TCRs B11 and B15 showed similarly strong activation of NFAT.

Overall, we reveal the TCR repertoire in naive antigen-specific precursor populations to be highly skewed in their functionality, with the majority of TCRs showing no or very low functional avidity, and only a small fraction of highly functional TCRs.

### Selective clonal expansion is governed by clear TCR avidity thresholds

To investigate the capability of clonotypes of different functional avidities to expand upon antigen encounter *in vivo*, we adoptively transferred 50 naive CD8<sup>+</sup> T cells of a single clonotype (for each TCR from the naive repertoire separately) into C57BL/6 recipient mice and analyzed these at day 8 after infection with Lm-SIINFEKL (Figures 4A and 4B). We observed strong clonal expansion during the acute phase of the primary immune response for the TCRs B11 and B15, as predicted by their structural and functional avidity (Figure 4B). TCR B3, which showed the highest antigen sensitivity without a detectable  $k_{off}$  rate, was also efficiently recruited (i.e., activated progeny cells could be detected) into the primary immune response, although clonal abundance was reduced. In this setting, we were unable to identify clonally expanded populations for the majority of transferred TCRs (Figure 4B). In line with high clonal expansion and TCR avidity, TCR B11 displayed the most effector differentiated phenotype, followed by TCR B15 and B3, which showed a larger fraction of memory precursors (Figure S4A).

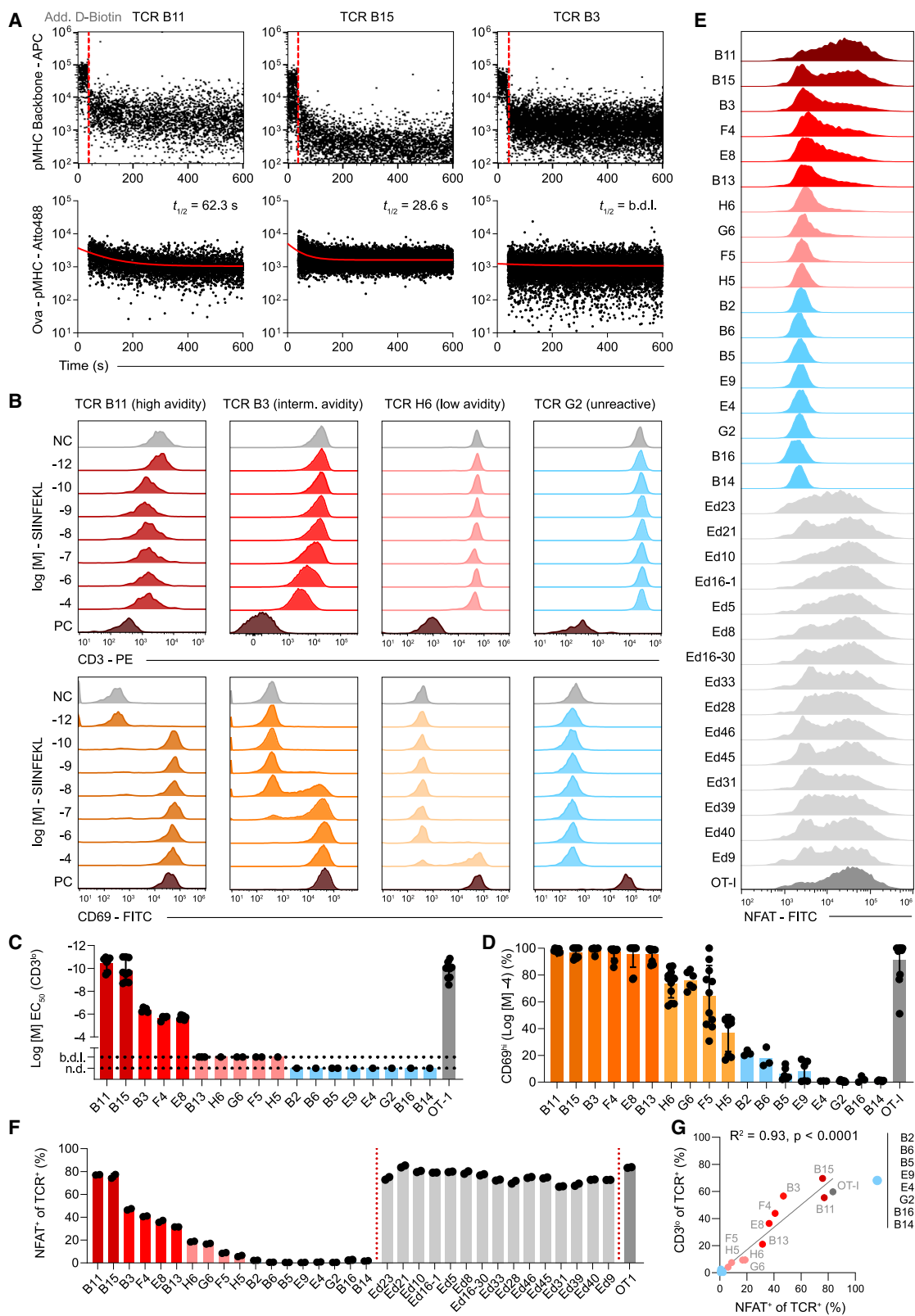
TCR avidity is a main driver of effective T cell recruitment. However, T cell priming *in vivo*—leading to activation and recruitment—underlies stochastic processes and can be influenced by the precursor size of a clonotype. We therefore increased the transferred monoclonal population size to 500 naive CD8<sup>+</sup> T cells per recipient and challenged C57BL/6 mice with Lm-SIINFEKL (Figures 4C and S4B). This time, we found primed and expanded T cell populations also for low-avidity TCRs (Figures 4D and S4C). However, phenotypic differences pointed to differences in the amount and strength of antigenic priming events. While for TCR B3 all recovered cells upregulated CD44

(E) Staining of TCR B11 after re-expression in retrogenic mice, representative of 12 independent experiments. Left: expression of congenic marker CD45.1; right: H-2K<sup>b</sup>/SIINFEKL-multimer staining (red) compared with an unspecific multimer (H-2K<sup>b</sup>/M38<sub>316-323</sub>, gray).

(F) Representative histograms of H-2K<sup>b</sup>/SIINFEKL-multimer staining of all identified TCRs from a single C57BL/6 mouse re-expressed in individual mice of 2–12 independent experiments. Multimer staining of OT-I T cells as reference (n = 8). Individual histograms were pooled from individual retrogenic mice and overlaid using the same scale.

Statistical testing was done using a two-sided Mann-Whitney test. \*\*\*\*p < 0.00001, \*\*\*p < 0.0001. Data in (C) and (D) are pooled from 11 and 7 independent experiments, respectively.

See also Figure S2.



(legend on next page)

and displayed effector differentiation to a large extent, TCRs of lower avidity such as TCR F4 showed variable activation and differentiation patterns (Figure 4E). Following the determined gradient of decreasing TCR avidity, we found an increasing number of T cells that remained in a naive (CD44<sup>lo</sup>) state (Figure 4F). Analogously, we identified a significant correlation between TCR functional avidity and clonal expansion (Figure 4G).

T cell recruitment and clonal expansion may also be influenced by TCR competition and access to antigen-presenting cells, so we selectively transferred monoclonal populations (50 cells) into Tcra<sup>-/-</sup> recipients (Figure S4D). TCR B15 and B3 showed comparable expansion in Tcra<sup>-/-</sup> as in WT recipients. Small clonally expanded populations of TCR E8 were visible in Tcra<sup>-/-</sup> but not in WT recipients. For TCRs with lower antigen sensitivity, progeny remained undetectable (Figure S4D).

These observations show that efficient TCR recruitment and clonal expansion during a primary infection are governed by clear avidity thresholds, which are only mildly influenced by competition effects.

### Individual low-avidity TCRs for the cognate SIINFEKL epitope can recognize mutant epitopes with high avidity

Having established avidity thresholds for efficient recruitment and clonal expansion *in vivo*, we wondered whether low-avidity TCRs of antigen-specific precursor populations might recognize mutated forms of the identified “cognate” epitope with higher avidity. Since we observed a strong correlation between the antigen-specific activation JTPRs and primary murine T cells (Figure 3D), we utilized the high-throughput compatibility of the JTPR model to assess a broad reactivity landscape of TCR repertoires. We first measured NFAT expression after incubation with the altered peptide ligands (APLs) SIYNFEKL (Y3) and SIITFEKL (T4) and observed a stark decrease in avidity across the repertoire, compared with SIINFEKL (N4) (Figure 5A). However, TCR E8 showed to be more responsive to the Y3 mutation (60.6% NFAT<sup>+</sup>) than to the cognate epitope N4 (36.4% NFAT<sup>+</sup>). This change in reactivity is relevant since previous data revealed the reactivity of TCR B3 (46.9% NFAT<sup>+</sup> when stimulated with N4) to represent the threshold for consistent *in vivo* recruitment and clonal expansion of naive T cells (Figure 4). We confirmed these cross-reactive events by stimulation of primary murine T cells and found recurrent correlation with antigen-specific activation of JTPRs (Figure S5A).

Based on the Y3 and T4 APL data, we set out to systematically dissect whether shifts in avidity against mutated forms of the epitope (such as for E8 in Figure 5A) are a general feature of low-avidity clonotypes (i.e., avidity values are lower against any or most altered epitopes), or whether absolute reactivity sizes are maintained while epitope hierarchies are changed (i.e., avidity values are similar, but different epitopes are recognized with high avidity). To this end, we generated an APL library consisting of 152 unique mutations of the N4 peptide, with each single amino acid being exchanged for any other amino acid at a time (Table S3). We thereby measured 5,016 unique TCR-pMHC interactions in JTPR after individual incubation with mutated peptides and characterized the avidity landscape in naive and antigen-experienced repertoires (Figures 5B–5D and S5B). This revealed a strong correlation between reactivity toward the cognate epitope and mutant epitopes for TCRs identified from the naive repertoire (Figures 5D and S5C; note that TCRs are ordered according to TCR reactivity against N4). This effect became even more pronounced when we analyzed a memory repertoire in the same manner (Figures S5B and S5D).

Accordingly, the high-avidity TCRs B11 and B15 most often displayed the highest reactivity against APLs (Figure 5D). However, for several individual APLs, other TCRs showed the highest reactivity, such as low-avidity TCR B2 against APL I1 (Figure 5D, light green TCR highlighted on the right) or TCR E8—which previously stood out because of its high reactivity against the often-studied APLs Y3 and T4 (Figure 5A). In conclusion, high reactivity against the cognate epitope N4 is often predictive of reactivity against other APLs, but we also detected several cases in which TCRs with low avidity against N4 were the strongest responders against a mutation (e.g., E8-Y3; E8-P4; B3-V6).

The effect of exchanged amino acids on the activation of high-avidity TCRs was mostly position dependent and less influenced by the exchanged amino acid itself. Mutations in positions 2, 5, and 8 barely affected recognition and functional avidity for TCRs B11 and B15 and TCRs from the antigen-experienced repertoire, whereas mutated positions 3, 4, 6, and 7 led to variable activation (Figures 5D and S5B). The crystal structure of the H-2K<sup>b</sup>/SIINFEKL complex has been previously reported and revealed differential accessibility of the peptide positions for TCR interactions.<sup>38</sup> Positions 4, 6, and 7 are highly accessible to pMHC-TCR binding—in line with the variable reactivity in our data—whereas positions 2, 5, and 8 are mainly buried in the

### Figure 3. TCR avidity distribution of antigen-specific precursor populations in naive donors is highly skewed

- (A) Mean dissociation kinetics during flow cytometric pMHC-TCR  $K_{off}$ -rate measurement of TCRs B11, B15, and B3; data are representative of 2 independent experiments. Upper panels: dissociation of the Strep-Tactin backbone after addition of D-biotin; lower panels: mean dissociation of monomeric pMHC molecules; b.d.l., below detection limit.
- (B)  $1 \times 10^6$  splenocytes of TCR retrogenic mice were stimulated with SIINFEKL peptide ranging from  $c = 10^{-4}$ – $10^{-12}$  M for 18 h. Histograms depict dose-dependent downregulation of the TCR-CD3 complex or upregulation of CD69.
- (C) Antigen sensitivity toward H-2K<sup>b</sup>/SIINFEKL after TCR re-expression in retrogenic mice. OT-I for comparison.
- (D) T cell activation (CD69 upregulation at  $10^{-4}$  M peptide dose) after TCR re-expression in retrogenic mice.
- (E) NFAT expression of JTPR after TCR re-expression and antigen-specific stimulation; naive repertoire: red and blue, educated repertoire: light gray (“Ed...”), and OT-I: dark gray.
- (F) Quantification of data shown in (E) of two technical replicates; bars depict mean.
- (G) Correlation between percentage of CD3<sup>lo</sup> primary murine T cells and percentage of NFAT<sup>+</sup> JTPR after antigen-specific stimulation; x axis: mean of data in (F) and y axis: mean of data in (C). Data in (B) are representative of at least 2 independent experiments ( $n = 2$ –4). Data in (C) and (D): each dot represents measurement of  $n = 1$ –4 independent experiments. TCRs are color-coded and ordered according to their functional avidity from dark red or orange (high avidity, based on CD3 downregulation or CD69 upregulation) to light red or orange (low avidity) to light blue (low avidity, defined through no detectable CD3 downregulation).
- See also Figure S3.

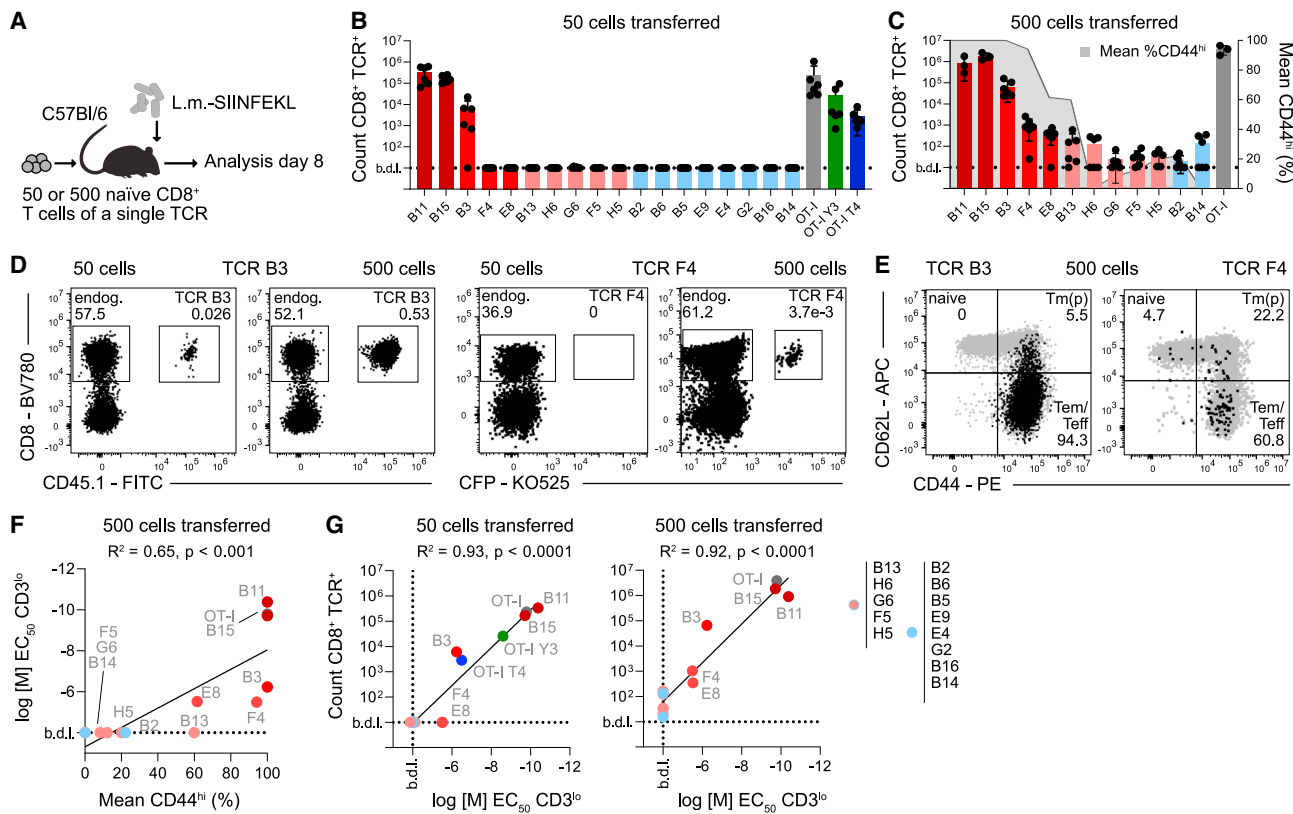


**Figure 4. Selective clonal expansion is governed by clear TCR avidity thresholds**

(A) Adoptive transfer of 50 or 500 naïve CD8<sup>+</sup> T cells of a single TCR into C57BL/6 mice, followed by infection with 5,000 colony-forming units (CFUs) of Lm-SIINFEKL.

(B) Recovered progeny after adoptive transfer of 50 naïve CD8<sup>+</sup> T cells in spleen on day 8 p.i. Progeny of 50 naïve OT-I cells after infection with Lm-SIINFEKL (N4, gray), -SIYNFEKL (Y3, green), and -SIITFEKL (T4, blue) for comparison.

(C) As in (B), but after transfer of 500 naïve CD8<sup>+</sup> T cells (left y axis); right y axis: mean percentage of recovered CD44<sup>hi</sup> T cells (gray line).

(D) Dot plots depict progeny when 50 or 500 naïve CD8<sup>+</sup> T cells expressing TCR B3 (left) or TCR F4 (right) were transferred ( $n = 6$ ).

(E) Dot plots show marker expression by transferred T cells as shown in (D), representative of 6 independent experiments.

(F) Scatter dot plot depicts correlation between EC<sub>50</sub> (% CD3<sup>lo</sup>) as shown in Figure 3E and mean percentage of CD44<sup>hi</sup> T cells as in (C).

(G) Scatter dot plots depict correlation between EC<sub>50</sub> (% CD3<sup>lo</sup>) and mean T cell clone recovery as in (B) and (C) in spleen after transfer of 50 cells (left) or 500 cells (right). Data in (B) and (C) are pooled from 19 and 11 independent experiments, respectively;  $n = 6$  mice per group (except in C, for B11, B15, and OT-I  $n = 3$  mice per group); b.d.l., below detection limit.

See also Figure S4.

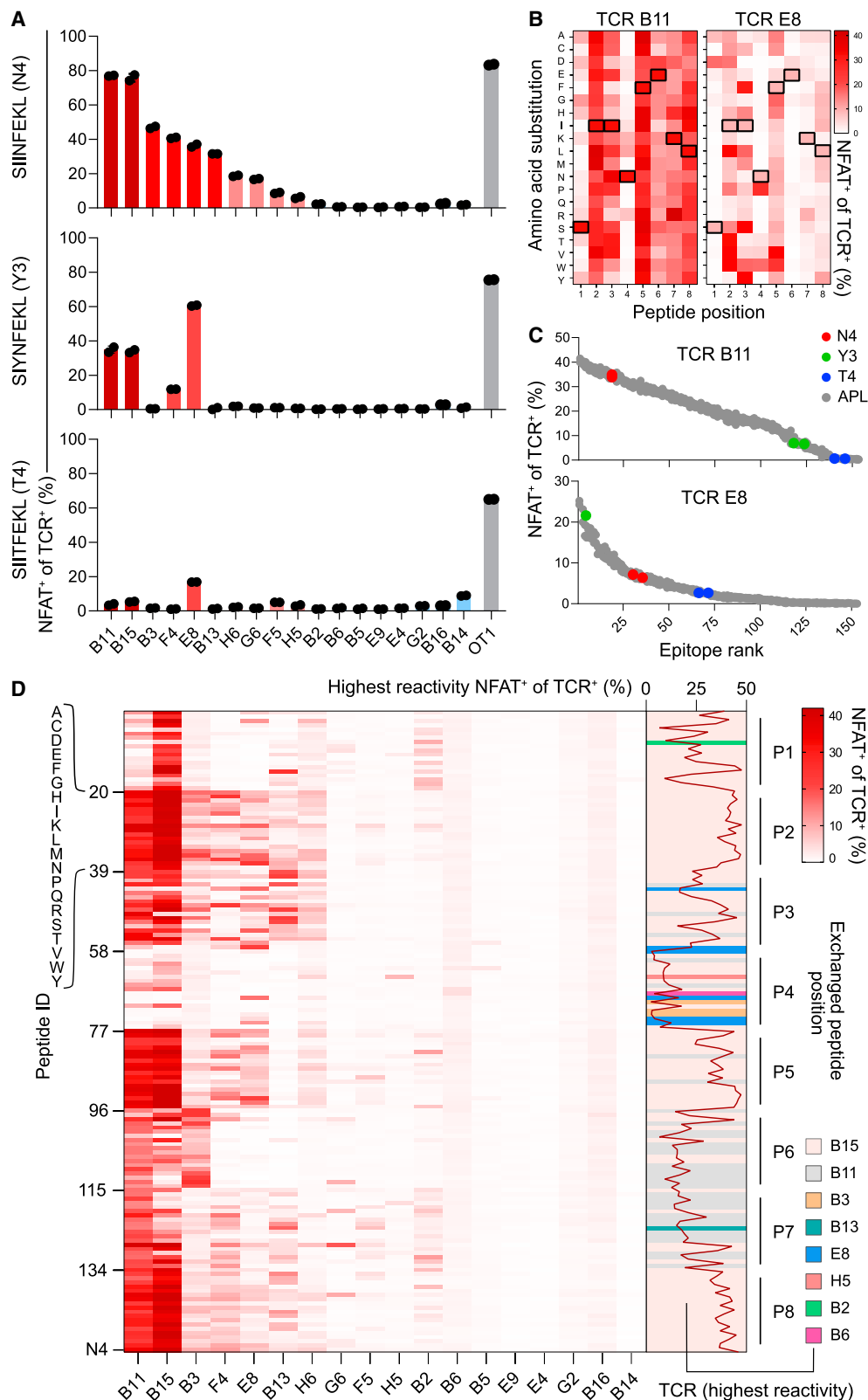
MHC binding groove, consistent with a decreased effect of mutations at these positions on antigen reactivity. Bentzen and colleagues have reported via DNA-barcoded pMHC complexes the reactivity spectrum of the OT-I receptor and have identified comparable results to our observations.<sup>39</sup> Accordingly, we observed a statistically significant correlation between our assessed reactivity and pMHC binding, as assessed by Bentzen et al. However, in many cases strong pMHC binding did not reflect strong T cell activation ( $R^2 = 0.56$  or  $R^2 = 0.40$ , depending on the employed peptide concentration; Figure S5E). Further, we observed that mutations at pMHC anchor positions still allowed for pMHC-TCR interactions and led to T cell activation, although these mutations were not predicted to bind (Figure S5F).

Overall, we identify several pMHC-TCR interactions (especially in the highly variable positions 1, 3, 4, 6, and 7) in which the repertoire response would be mainly driven by a single TCR for both the naïve and educated repertoire (Figure S5G).

Most of these mutations are recognized by either of the high-avidity TCRs (i.e., B11 and B15). However, several mutations in these key positions also lead to highly effective activation of TCRs from the lower-avidity spectrum (Figures 5D and S5G).

#### Polyclonal repertoires can provide enhanced protection against mutational escape mechanisms

To investigate how differential avidities against a cognate epitope—but also the mutational avidity landscape—of polyclonal precursor populations translate into recruitment and expansion after infection *in vivo*, we “rebuilt” a representative naïve repertoire for polyclonal adoptive transfer experiments. We sorted and simultaneously transferred small populations (50 cells for each TCR) of color-barcoded naïve CD8<sup>+</sup> T cells comprising 10 unique clonotypes of different avidities into Tcra<sup>-/-</sup> recipients (Figures 6A and 6B). Upon Lm-N4 infection, we tracked the barcoded TCR populations in peripheral blood

**Figure 5. Individual low-avidity TCRs for the cognate SIINFEKL epitope can recognize mutant epitopes with high avidity**

(A) NFAT expression in JTPR after stimulation with SIINFEKL (N4)-peptide (top, as in Figure 3F) and altered peptide ligands (APLs) SIYNFEKL (Y3, middle) and SIITFEKL (T4, bottom).

(legend continued on next page)

over time and analyzed spleens after primary infection and after homologous (Lm-N4) or heterologous (Lm-Y3) secondary infection (Figure 6C). Analogous to the hierarchies derived from monoclonal transfers (Figure 4), the high-avidity clones B11 and B15 dominated the primary immune response upon poly-clonal transfer (d7) (Figures 6C, 6D, and S6A). In contrast to peripheral blood, we observed consistent recruitment (in 6/6 recipients) for TCR B3 in spleens (Figure S6B). We observed partial recruitment into the primary response of lower-avidity TCRs with decreasing antigen sensitivity, e.g., in 4/6, 3/6, and 1/6 recipient spleens for TCRs F4, E8, and B13, respectively (Figures 6D and S6B). The immune response contracted over time, but we consistently recovered high-avidity TCR B11 and B15 cells (Figure 6D).

Upon homologous recall with Lm-N4, we observed differences in clonal expansion between TCR B11 (mean: 72.2% of T cells in blood) and B15 (mean: 27.7%; Figures 6D, S6A, and S6B) and little recruitment of lower avidity clones. Overall, homologous rechallenge with the same epitope revealed a clear fine-tuning of the memory immune response with an accentuated advantage of the highest avidity clonotype in secondary infections. Of note, B11 and B15 did not show differences in antigen sensitivity (Figure 3); however, TCR B11 displayed an increased  $k_{off}$  rate compared with B15.

Upon heterologous rechallenge with Lm-Y3, we observed contraction of TCR B11 and B15 cells (Figure 6D), in line with the fact that these clonotypes did not recognize Y3 with high avidity (Figure 5A). Instead, TCR E8 dominated the secondary immune response against Y3 with a mean recovery of 55.0% of transgenic T cells in blood, while TCR E8 T cells had not been detectable after Lm-N4 recall (Figure 6D). The high antigen sensitivity toward the Y3 epitope for TCR E8 (Figures 5A and 6E) therefore conferred a selective advantage, resulting in clonal expansion and dominance upon secondary infection—even though it developed from a small memory population—and had to compete against large numbers of memory cells harboring TCRs B11 and B15 (Figure 6D), which recognize Y3 with lower avidity (Figure 5A). Consistent with these results, we did not observe quenching of a high-avidity immune response in the presence of large numbers of lower-avidity T cells recognizing the same epitope (Figure S6C). To investigate this further, we adoptively co-transferred 50 naive CD8<sup>+</sup> T cells of TCR B11 alongside increasing numbers of TCR B3 (50, 500, 5,000) into WT or Tcra<sup>-/-</sup> recipients. After infection with Lm-N4, we did not identify significant differences between clonal expansion of B11 in the presence of B3 cells of any number and irrespective of the recipient system (Figure S6D). However, we did observe increased recruitment of TCR B3 in both WT and Tcra<sup>-/-</sup> recipients with larger transferred populations (Figure S6D).

Following the differential recruitment of TCR E8 cells, depending on the recall epitope, we investigated the functional relevance of TCRs that respond with low avidity against cognate epi-

topes but are recalled with high avidity against mutated epitopes. We transferred an oligoclonal TCR repertoire consisting of high-avidity TCR B11 and intermediate-avidity TCR B3 in combination with (group I) or without (group II) TCR E8 into Tcra<sup>-/-</sup> mice (Figure 6F). Recipients were initially immunized with MVA-OVA expressing the N4 epitope and later challenged with Lm-N4 or -T4. This setting reflects a scenario in which vaccination with a WT strain is followed by an infection with a pathogen that has or has not mutated an immunodominant target epitope. This time, we chose the T4 instead of the Y3 variant since T4 is associated with a complete loss of reactivity for almost all of the identified N4-reactive naive repertoire, except for TCR E8, which maintains reactivity (Figure 5A).

After vaccination, TCR B11 dominated the acute (mean: (I) 99.9% and (II) 99.7% of T cells in blood) and memory (mean: (I) 97.7% and (II) 95.5%) phases of the immune response (Figure S6E). We observed variable degrees of clonal expansion for TCR B3 (detectable progeny in 66.7% of recipients, n = 24) and TCR E8 (detectable progeny in 41.6% of recipients, n = 12) in peripheral blood during the acute phase. Upon secondary infection with Lm-N4, we detected increased clonal expansion in blood for TCR B3 with recovered clones in 75% (91% in spleen, n = 12) and for TCR E8 with recovered clones in blood and spleen in 100% (n = 6) of recipients (Figures 6G, 6H, and S6E). We did not observe significant differences in clonal expansion for TCR B3 and B11 in the presence or absence of TCR E8. However, while TCR B11 was upon rechallenge the most dominant TCR, B11 T cells were significantly less expanded when rechallenged with the T4 variant, compared with the N4 variant.

This differential expansion of B11 T cells translated into different levels of protection against bacterial infection (Figure 6I). High amounts of TCR B11 T cells upon N4 rechallenge (reacting to N4 with high avidity) mediated complete protection against Lm-N4, irrespective of the presence or absence of TCR E8. In contrast, upon T4 rechallenge, low amounts of TCR B11 T cells (reacting to T4 with low avidity) resulted in loss of protection against Lm-T4 when TCR E8 T cells were not present, with 6/6 mice showing bacteria in the liver. When TCR E8 was present, however, protection could be almost completely restored through recall of TCR E8 T cells through the T4 variant (Figure 6I). The protective effect of TCR E8 upon Lm-T4 recall was most likely derived from memory cells induced by MVA-OVA (N4) priming, as mice that did not receive prior immunization, but the same number (i.e., 50) of naive E8 T cells and the same dose of Lm-T4 failed to control bacterial infection (Figures S6F and S6G) and showed equal amounts of bacteria as control mice that received no T cells at all (Figure S6H).

Overall, these data demonstrate that recruitment of broad TCR repertoires enables flexible secondary immune responses, in which TCRs that recognize the initial cognate epitope with low avidity can play a decisive role in protective immunity upon heterologous rechallenge.

(B) Peptide stimulation with APL library: JTPR were stimulated with 152 APLs with single-position mutations of N4; black squares depict unmutated SIINFEKL.

(C) Data from (B) as scatter dot plot. APLs are ordered by measured NFAT expression (epitope rank) from highest to lowest.

(D) Data as described in (B) as combined heatmap. APLs are ordered by mutated position (from P1 to P8, right) and exchanged amino acid (left). Line plot depicts highest measured NFAT expression over the whole repertoire (red line, right); background coloring shows the TCR with the highest reactivity. Data in (D) are pooled from 18 independent experiments; NFAT expression is displayed as the mean of two technical replicates.

See also Figure S5.

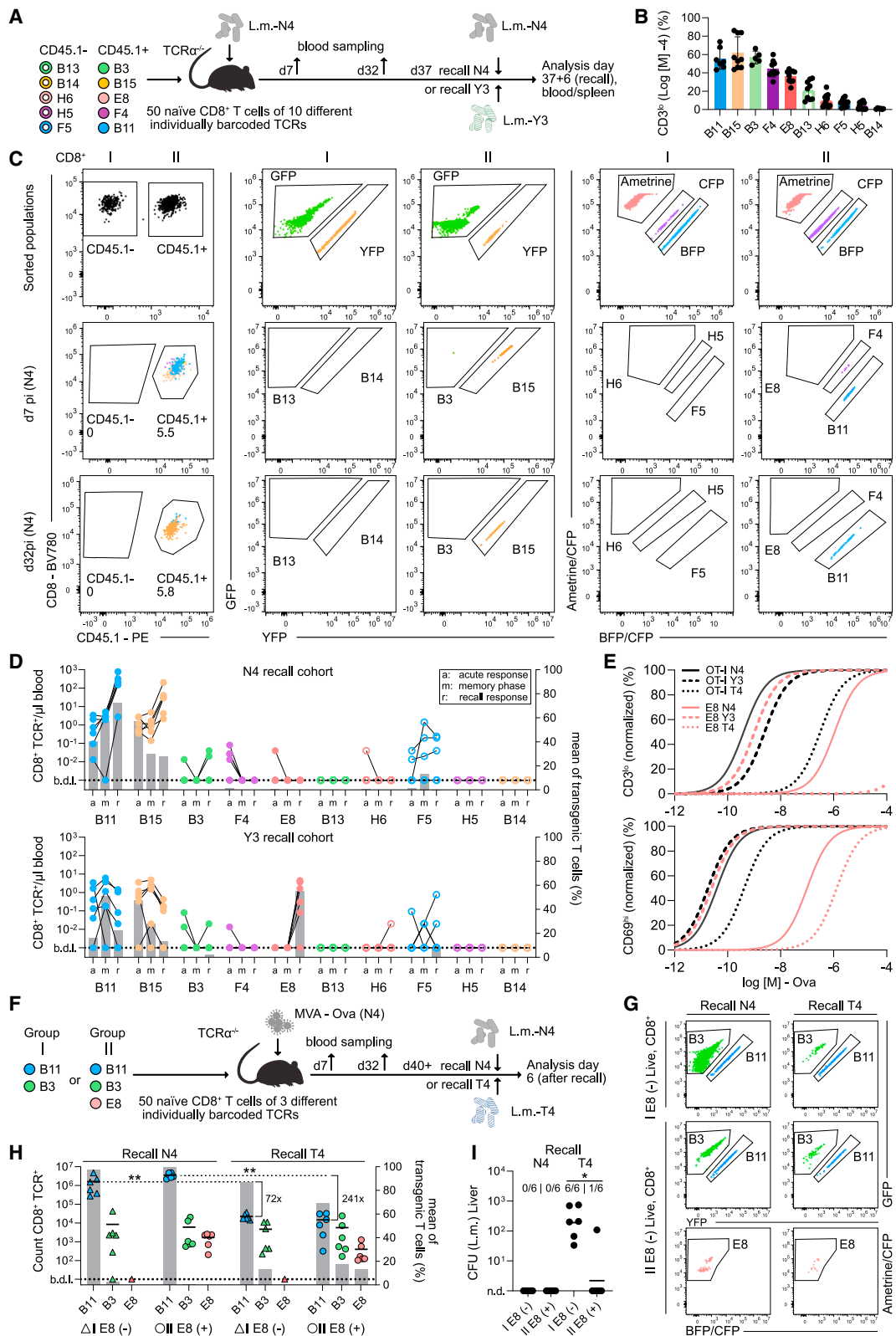


**Figure 6. Polyclonal repertoires provide enhanced protection against mutational escape mechanisms**

(A) Schematic: TCR populations were barcoded with a unique combination of CD45.1/45.2 and GYACB fluorescent proteins and co-transferred. (B) T cell-avidity distribution of transferred polyclonal TCR repertoire as shown in Figure 3B.

(legend continued on next page)

## DISCUSSION

The physiological role of low-avidity T cell clones is not well understood. Novel technologies allow us now to study the recruitment of polyclonal TCR repertoires from the naive compartment in so far unmatched detail.

Our single-cell analyses of 40 endogenous polyclonal repertoires upon infection with Lm-SIINFEKL revealed variable *in vivo* activation of up to 100 unique T cell clones, with clonal dominance of only 2–3 clonotypes. These findings were independent from whether antigen-reactive T cells were defined through pMHC multimer binding or through expression of an antigen-reactive gene score. Consistent with these results, it has recently been shown for CD4<sup>+</sup> T cells that 100–160 clones per mouse are recruited into a GP<sub>66–77</sub> epitope-specific response, with only 7–10 clones accounting for 50% of the total population size.<sup>19</sup> At the same time, the endogenous precursor population for our model antigen SIINFEKL has been described to encompass up to 170 T cells in an entire mouse,<sup>6</sup> which we estimate in our study to be likely twice the size. We here, and others before<sup>40</sup> us, report that the naive TCR repertoire is almost perfectly diverse. Our findings imply that an astonishing amount of this repertoire is initially recruited *in vivo*, as previously investigated on a population level for different specificities.<sup>8</sup> We identify that initial recruitment comprises many low-avidity TCRs and only a small fraction of high-avidity clones.

Comparing the precursor size with the clonal distribution in the primary immune response, we estimate the proportion of high-avidity clones to be less than 1 in 100 antigen-reactive T cells of the same specificity. Previous studies have already suggested this through TCR-repertoire diversity analysis,<sup>16,17,41</sup> investigations with a limited number of *in vitro* expanded T cell clones,<sup>9</sup> CD8-null pMHC multimers,<sup>4</sup> TCR signaling reporter assays,<sup>20</sup> and 2D affinity measurements.<sup>10</sup> We provide experimental proof of this concept by analyzing the avidity distribution of a naive repertoire through transgenic re-expression and functional characterization of identified TCRs, which showed an overwhelming abundance of low-avidity clonotypes in the precursor repertoire, and we demonstrated precise avidity thresholds for the recruitment and clonal expansion of T cells. These thresholds differ depending on cellular precursor frequency and phenotype.

While we confirmed previous observations that the recruitment of high-avidity clones is highly efficient,<sup>15</sup> we revealed that decreasing TCR avidity was associated with decreasing robustness of recruitment. Nevertheless, the overall avidity

threshold for initial recruitment into a primary immune response seems to be remarkably low. Our experimental data show that the threshold for responses to H2-K<sup>b</sup>/SIINFEKL lies at the avidity level of the OT-I T4 interaction, which has been previously described to mark the avidity threshold for positive selection in the thymus.<sup>42</sup>

What could be the physiological relevance of the here identified low avidity thresholds for the initial recruitment of T cells? A high avidity threshold for T cell activation *in vivo* would result right from the beginning in a narrow, oligoclonal immune response, which nevertheless should be highly effective in eliminating a pathogen. However, a narrow primary T cell response would not provide broad flexibility to counteract mutational escape. It has been proposed that TCR diversity in immune responses is beneficial for long-term protection against infection, especially in the case of pathogens with high mutation rates.<sup>43,44</sup> So far, these studies followed endogenous immune responses on a population level. We here confirmed the narrowing of the -immune repertoire upon homologous secondary infection, which selects for the highest avidity response,<sup>13,44</sup> in a traceable, polyclonal repertoire. We thereby directly show the functional significance of polyclonal T cell responses, which provide a buffer against heterologous infections.

In line with previous reports, we found low-avidity TCRs to be capable of forming small memory populations after infection.<sup>22,44</sup> Whereas single naive T cells show extraordinary capacities in burst size and are fully able to reconstitute unrestricted immunity,<sup>33</sup> T central memory cells (T<sub>CM</sub>) show similar stem-like properties<sup>45</sup> but are able to supersede naive T cells in response time to infection.<sup>46</sup> In our study, we provide experimental evidence that memory T cells with low avidity against the “cognate” WT epitope are capable of expanding upon encounter with a mutated antigen that is recognized with high avidity, despite the presence of a large competing memory population (with lower avidity against the mutated antigen). This indicates that a benefit of the recruitment of a polyclonal T cell repertoire upon primary infection could lie in the generation of a flexible “niche” of TCRs that can mediate enhanced protective-ty upon heterologous secondary responses. Viral escape through T cell epitope mutations was demonstrated more than 30 years ago,<sup>47</sup> and selective expansion of cross-reactive CD8<sup>+</sup> T cells by influenza variants has been observed before.<sup>48</sup> In this report, we systematically dissected the cross-reactivity landscape of TCRs derived from naive precursor and antigen-experienced repertoires. Although we observed a correlation between high TCR avidity against the cognate epitope and its

(C) Dot plots depict tracking of barcoded CD8<sup>+</sup> T cells; upper panels: sorted T cells dissected according to their combinatorial expression of CD45.1 (CD45.1– group I and CD45.1+ group II) and GYACB; middle panels: recovered T cells at day 7 p.i. in blood; lower panels: recovered T cells at day 32 p.i. (memory phase).  
(D) Scatterplots depict recovered T cells in blood per  $\mu\text{L}$  (left y axis) at three time points; a, acute (day 7 p.i.); m, memory phase (day 32 p.i.); r, recall (day 6 p.i. secondary infection); bars show mean fraction of recovered T cells (right y axis); upper panels: Tcra<sup>-/-</sup> rechallenged with Lm-N4; lower panels: Tcra<sup>-/-</sup> re-challenged with Lm-Y3.

(E) Antigen sensitivity of TCR E8 and OT-I toward H-2K<sup>b</sup>-N4, -Y3, and -T4 after re-expression in retrogenic mice.  
(F) Schematic: co-transfer of TCR B11 and B3 (group I) or additionally TCR E8 (group II) into Tcra<sup>-/-</sup> followed by immunization with  $1 \times 10^7$  plaque-forming units (PFUs) of MVA-OVA (N4). Secondary infections were performed with 20,000 CFU of Lm-N4 or -T4.  
(G) Dot plots depict recovery of T cells from spleen at day 6 post challenge with Lm-N4 (left, n = 6) and Lm-T4 (right, n = 6).  
(H) Recovered progeny in spleen (left y axis) after challenge with Lm-N4 or -T4; right y axis: mean percentage of CD44<sup>hi</sup> T cell clones (gray bars).  
(I) CFU of Lm isolated from liver of recipients after secondary infection. See also Figure S6.  
Data in (C) and (G) are representative of 6 mice, respectively. Data in (B) and (E) depict mean of n = 1–4 independent experiments. In (F), (H), and (I): n = 6 mice per group. Statistical testing was done using a two-sided Mann-Whitney test. \*p < 0.05 and \*\*p < 0.01.

related APLs, there are still numerous mutations that abrogate its recognition. Even though these may be rare cases in a polyclonal repertoire, we identified several low-avidity clonotypes that are able to fill “gaps” in the reactivity landscape of high-avidity TCRs, which are crucial for protection from heterologous secondary infections.

There is a controversial discussion about the functional role of low-<sup>49</sup> and high-avidity<sup>37,50,51</sup> T cells, especially in mediating tumor protection. So far, many studies already concluded that effective protection from viral infections is mainly established by high-avidity T cells.<sup>52–54</sup> Whereas this might be true for resolving acute infections, during chronic antigen exposure—as in chronic infections or cancer—intermediate- and low-avidity T cells seem to be less prone to dysfunctionality programs (like immunosenescence or exhaustion) and could become most relevant for control of disease. Of note, although the number of low-avidity T cell clones recruited into immune responses largely exceeds the few high-avidity clones present in the naive repertoire, they seem not to interfere with the priming and dominant expansion of high-avidity clonotypes. Previous studies suggest that the presence of low-avidity T cells in some tumor diseases inhibits T cell effector function by competing for pMHC access.<sup>55,56</sup> However, in our experimental setting, we did not observe any impairment in recruitment or clonal expansion of high-avidity T cells upon bacterial infection, even when low-avidity clones were present at 100-fold higher numbers. Jenkins and colleagues previously demonstrated that a large excess of high-avidity T cells can inhibit the recruitment of smaller precursor populations directed toward the same epitope.<sup>57</sup> Nevertheless, this effect was diminished in the range of a more physiological distribution of antigen-reactive T cell clones, and it supports the hypothesis that recruitment of CD8<sup>+</sup> T cell repertoires from the naive compartment are largely independent of one another. In our study, recruitment of lower-avidity T cells was not inhibited by the presence of high-avidity clonotypes but increased according to precursor frequencies. Although the increase appeared to be independent of interclonal competition, it was also not strictly linear, suggesting stochastic avidity-dependent thresholds for *in vivo* priming and expansion. Nevertheless, it is possible that other factors in the tumor environment regulate the interplay of polyclonal populations, compared with infectious diseases.

Overall, our data provide an integrated framework on how polyclonal antigen-reactive T cell responses develop from scratch in a TCR avidity-dependent manner. In terms of clinical relevance, our findings argue that T cell therapies with T cells expressing transgenic TCRs should be considered to entail polyclonal products with high- and low-avidity TCRs. The deliberate use of cross-reactive TCRs for transgenic T cell products to counteract pathogen heterogeneity has been previously proposed, e.g., for therapy of hepatitis C.<sup>58</sup> Furthermore, vaccine design should not focus solely on the induction of high-avidity oligoclonal responses but also on the induction of polyclonality—even within single-antigen specificities. Finally, the here identified and functionally characterized TCRs that are representative of an antigen-reactive precursor repertoire, as well as the establishment of an *in vivo* traceable polyclonal population with single-TCR resolution, are a generically useful resource for studying antigen-reactive T cell responses.

## Limitations of the study

This study reveals novel aspects of avidity-dependent development and maintenance of polyclonal CD8<sup>+</sup> T cell responses. Although extensive, our analyses are limited to mouse models and focus on a single-epitope specificity (SIINFEKL) in acute infection or upon vaccination. Additional studies are necessary to establish whether our conclusions can be generalized to other epitope specificities, CD4<sup>+</sup> T cells, and to immune responses in humans.

## STAR★METHODS

Detailed methods are provided in the online version of this paper and include the following:

- KEY RESOURCES TABLE
- RESOURCE AVAILABILITY
  - Lead contact
  - Materials availability
  - Data and code availability
- EXPERIMENTAL MODEL AND SUBJECT DETAILS
  - Mice
  - Cell lines
- METHOD DETAILS
  - Infections
  - Generation of retroviruses
  - Generation of T cell retrogenic mice
  - Flow cytometry
  - Peptide-MHC (pMHC) multimer staining
  - Speed enrichment and single-cell sorting
  - Single-cell PCR
  - Adoptive transfer and tracking of T cells
  - Flow-cytometry-based TCR-ligand  $k_{off}$ -rate
  - Antigen-specific activation of primary T cells
  - *In vivo* L.m. OVA proliferation
  - Antigen-specific activation of human JTPR
  - Quantification of colony forming units (CFUs)
  - Antigen-specific activation for single-cell RNA sequencing
  - Single-cell RNA sequencing
  - scRNA-seq data analysis
  - Clonotype definition from single-cell RNA sequencing data
  - TCR DNA template design
- QUANTIFICATION AND STATISTICAL ANALYSES

## SUPPLEMENTAL INFORMATION

Supplemental information can be found online at <https://doi.org/10.1016/j.immuni.2023.04.010>.

## ACKNOWLEDGMENTS

We thank members of the Busch laboratory for experimental help and critical discussion. We also thank Sine Reker Hadrup and Amalie Bentzen (Technical University of Denmark) for providing the raw data values of OT-I APL pMHC binding.

This work was supported by the Deutsche Forschungsgemeinschaft (DFG) (SFB 1054/3 - 210592381 [projects B09 and B15], SFB-TRR 338/1 - 452881907 [projects A01 and B02], and SFB 1371 - 395357507 [project P04] to D.H.B. and K.S.) as well as the “European Research council starting grant” (SCIMAP) to V.R.B. K.S. is also supported by the German Federal Ministry of Education and Research (BMBF, 01KI2013).

## AUTHOR CONTRIBUTIONS

D.H.B. and K.S. conceptualized the study; A.S., S.G., D.H.B., and K.S. developed methodology; A.S. and K.S. developed and performed software analyses; A.S. and K.S. conducted formal analysis of the data; A.S., S.J., L.R., P.H., and K.I.W. performed experiments; V.R.B. and D.H.B. contributed resources; A.S., D.H.B., and K.S. wrote the manuscript; all authors read and approved the manuscript; D.H.B. acquired most of the funding; D.H.B. and K.S. supervised the study and administered the project.

## DECLARATION OF INTERESTS

D.H.B. is co-founder of STAGE Cell Therapeutics GmbH (now Juno Therapeutics/Celgene) and T Cell Factory B.V. (now Kite/Gilead). D.H.B. has a consulting contract with and receives sponsored research support from Juno Therapeutics/Celgene.

Received: November 15, 2022

Revised: February 1, 2023

Accepted: April 13, 2023

Published: May 9, 2023

## REFERENCES

- Jenkins, M.K., and Moon, J.J. (2012). The role of naive T cell precursor frequency and recruitment in dictating immune response magnitude. *J. Immunol.* 188, 4135–4140. <https://doi.org/10.4049/jimmunol.1102661>.
- Tscharke, D.C., Croft, N.P., Doherty, P.C., and La Gruta, N.L. (2015). Sizing up the key determinants of the CD8(+) T cell response. *Nat. Rev. Immunol.* 15, 705–716. <https://doi.org/10.1038/nri3905>.
- Alanio, C., Lemaitre, F., Law, H.K.W., Hasan, M., and Albert, M.L. (2010). Enumeration of human antigen-specific naive CD8+ T cells reveals conserved precursor frequencies. *Blood* 115, 3718–3725. <https://doi.org/10.1182/blood-2009-10-251124>.
- Legoux, F., Debeaupuis, E., Echasserieau, K., de La Salle, H., Saulquin, X., and Bonneville, M. (2010). Impact of TCR reactivity and HLA phenotype on naive CD8 T cell frequency in humans. *J. Immunol.* 184, 6731–6738. <https://doi.org/10.4049/jimmunol.1000295>.
- Neller, M.A., Ladell, K., McLaren, J.E., Matthews, K.K., Gostick, E., Pentier, J.M., Dolton, G., Schauenburg, A.J.A., Koning, D., Fontaine Costa, A.I.C.A., et al. (2015). Naive CD8+ T-cell precursors display structured TCR repertoires and composite antigen-driven selection dynamics. *Immunol. Cell Biol.* 93, 625–633. <https://doi.org/10.1038/icb.2015.17>.
- Obar, J.J., Khanna, K.M., and Lefrançois, L. (2008). Endogenous naive CD8+ T cell precursor frequency regulates primary and memory responses to infection. *Immunity* 28, 859–869. <https://doi.org/10.1016/j.immuni.2008.04.010>.
- Qi, Q., Liu, Y., Cheng, Y., Glanville, J., Zhang, D., Lee, J.Y., Olshen, R.A., Weyand, C.M., Boyd, S.D., and Goronzy, J.J. (2014). Diversity and clonal selection in the human T-cell repertoire. *Proc. Natl. Acad. Sci. USA* 111, 13139–13144. <https://doi.org/10.1073/pnas.1409155111>.
- La Gruta, N.L., Rothwell, W.T., Cukalac, T., Swan, N.G., Valkenburg, S.A., Kedzierska, K., Thomas, P.G., Doherty, P.C., and Turner, S.J. (2010). Primary CTL response magnitude in mice is determined by the extent of naive T cell recruitment and subsequent clonal expansion. *J. Clin. Invest.* 120, 1885–1894. <https://doi.org/10.1172/JCI41538>.
- Hombrink, P., Raz, Y., Kester, M.G.D., de Boer, R., Weißbrich, B., von dem Borne, P.A., Busch, D.H., Schumacher, T.N.M., Falkenburg, J.H.F., and Heemskerk, M.H.M. (2013). Mixed functional characteristics correlating with TCR-ligand off-rate of MHC-tetramer reactive T cells within the naive T-cell repertoire. *Eur. J. Immunol.* 43, 3038–3050. <https://doi.org/10.1002/eji.201343397>.
- Zhang, S.Q., Parker, P., Ma, K.Y., He, C., Shi, Q., Cui, Z., Williams, C.M., Wendel, B.S., Meriwether, A.I., Salazar, M.A., and Jiang, N. (2016). Direct measurement of T cell receptor affinity and sequence from naïve antiviral T cells. *Sci. Transl. Med.* 8, 341ra77. <https://doi.org/10.1126/scitranslmed.aaf1278>.
- Burnet, F.M. (1959). *The Clonal Selection Theory of Acquired Immunity* (Vanderbilt University Press).
- Lanzavecchia, A., and Sallusto, F. (2002). Progressive differentiation and selection of the fittest in the immune response. *Nat. Rev. Immunol.* 2, 982–987. <https://doi.org/10.1038/nri959>.
- Busch, D.H., and Palmer, E.G. (1999). T cell affinity maturation by selective expansion during infection. *J. Exp. Med.* 189, 701–710. <https://doi.org/10.1084/jem.189.4.701>.
- Savage, P.A., Boniface, J.J., and Davis, M.M. (1999). A kinetic basis for T cell receptor repertoire selection during an immune response. *Immunity* 10, 485–492. [https://doi.org/10.1016/S1074-7613\(00\)80048-5](https://doi.org/10.1016/S1074-7613(00)80048-5).
- van Heijst, J.W.J., Gerlach, C., Swart, E., Sie, D., Nunes-Alves, C., Kerkhoven, R.M., Arens, R., Correia-Neves, M., Schepers, K., and Schumacher, T.N.M. (2009). Recruitment of antigen-specific CD8+ T cells in response to infection is markedly efficient. *Science* 325, 1265–1269. <https://doi.org/10.1126/science.1175455>.
- Cukalac, T., Chadderton, J., Handel, A., Doherty, P.C., Turner, S.J., Thomas, P.G., and La Gruta, N.L. (2014). Reproducible selection of high avidity CD8+ T-cell clones following secondary acute virus infection. *Proc. Natl. Acad. Sci. USA* 111, 1485–1490. <https://doi.org/10.1073/pnas.1323736111>.
- Cukalac, T., Kan, W.T., Dash, P., Guan, J., Quinn, K.M., Gras, S., Thomas, P.G., and La Gruta, N.L. (2015). Paired TCR $\alpha\beta$  analysis of virus-specific CD8(+) T cells exposes diversity in a previously defined 'narrow' repertoire. *Immunol. Cell Biol.* 93, 804–814. <https://doi.org/10.1038/icb.2015.44>.
- Kedzierska, K., La Gruta, N.L., Turner, S.J., and Doherty, P.C. (2006). Establishment and recall of CD8+ T-cell memory in a model of localized transient infection. *Immunol. Rev.* 211, 133–145. <https://doi.org/10.1111/j.0105-2896.2006.00386.x>.
- Khatun, A., Kasmani, M.Y., Zander, R., Schauder, D.M., Snook, J.P., Shen, J., Wu, X., Burns, R., Chen, Y.G., Lin, C.W., et al. (2021). Single-cell lineage mapping of a diverse virus-specific naïve CD4 T cell repertoire. *J. Exp. Med.* 218. <https://doi.org/10.1084/jem.20200650>.
- Martinez, R.J., Andargachew, R., Martinez, H.A., and Evavold, B.D. (2016). Low-affinity CD4+ T cells are major responders in the primary immune response. *Nat. Commun.* 7, 13848. <https://doi.org/10.1038/ncomms13848>.
- Ozga, A.J., Moalli, F., Abe, J., Swoger, J., Sharpe, J., Zehn, D., Kreutzfeldt, M., Merkler, D., Ripoll, J., and Stein, J.V. (2016). pMHC affinity controls duration of CD8+ T cell-DC interactions and imprints timing of effector differentiation versus expansion. *J. Exp. Med.* 213, 2811–2829. <https://doi.org/10.1084/jem.20160206>.
- Zehn, D., Lee, S.Y., and Bevan, M.J. (2009). Complete but curtailed T-cell response to very low-affinity antigen. *Nature* 458, 211–214. <https://doi.org/10.1038/nature07657>.
- Schober, K., Voit, F., Grassmann, S., Müller, T.R., Eggert, J., Jarosch, S., Weißbrich, B., Hoffmann, P., Borkner, L., Nio, E., et al. (2020). Reverse TCR repertoire evolution toward dominant low-affinity clones during chronic CMV infection. *Nat. Immunol.* 21, 434–441. <https://doi.org/10.1038/s41590-020-0628-2>.
- Martinez, R.J., and Evavold, B.D. (2015). Lower affinity T cells are critical components and active participants of the immune response. *Front. Immunol.* 6, 468. <https://doi.org/10.3389/fimmu.2015.00468>.
- Sabatino, J.J., Huang, J., Zhu, C., and Evavold, B.D. (2011). High prevalence of low affinity peptide-MHC II tetramer-negative effectors during polyclonal CD4+ T cell responses. *J. Exp. Med.* 208, 81–90. <https://doi.org/10.1084/jem.20101574>.
- Fischer, D.S., Ansari, M., Wagner, K.I., Jarosch, S., Huang, Y., Mayr, C.H., Strunz, M., Lang, N.J., D'Ippolito, E., Hammel, M., et al. (2021). Single-cell RNA sequencing reveals ex vivo signatures of SARS-CoV-2-reactive T cells through 'reverse phenotyping'. *Nat. Commun.* 12, 4515. <https://doi.org/10.1038/s41467-021-24730-4>.

27. Becht, E., McInnes, L., Healy, J., Dutertre, C.A., Kwok, I.W.H., Ng, L.G., Ginhoux, F., and Newell, E.W. (2018). Dimensionality reduction for visualizing single-cell data using UMAP. *Nat. Biotechnol.* <https://doi.org/10.1038/nbt.4314>.
28. Traag, V.A., Waltman, L., and van Eck, N.J. (2019). From Louvain to Leiden: guaranteeing well-connected communities. *Sci. Rep.* 9, 5233. <https://doi.org/10.1038/s41598-019-41695-z>.
29. van der Geest, K.S.M., Abdulahad, W.H., Horst, G., Lorencetti, P.G., Bijzet, J., Arends, S., van der Heiden, M., Buisman, A.M., Kroesen, B.J., Brouwer, E., et al. (2015). Quantifying distribution of flow cytometric TCR-V $\beta$  usage with economic statistics. *PLoS One* 10, e0125373. <https://doi.org/10.1371/journal.pone.0125373>.
30. Plambeck, M., Kazeroonian, A., Loeffler, D., Kretschmer, L., Salinno, C., Schroeder, T., Busch, D.H., Flossdorf, M., and Buchholz, V.R. (2022). Heritable changes in division speed accompany the diversification of single T cell fate. *Proc. Natl. Acad. Sci. USA* 119. <https://doi.org/10.1073/pnas.2116260119>.
31. Holst, J., Vignali, K.M., Burton, A.R., and Vignali, D.A.A. (2006). Rapid analysis of T-cell selection in vivo using T cell-receptor retrogenic mice. *Nat. Methods* 3, 191–197. <https://doi.org/10.1038/nmeth858>.
32. Grassmann, S., Pachmayr, L.O., Leube, J., Mihatsch, L., Andrae, I., Flommersfeld, S., Oduro, J., Cicin-Sain, L., Schiemann, M., Flossdorf, M., and Buchholz, V.R. (2019). Distinct surface expression of activating receptor Ly49H drives differential expansion of NK cell clones upon murine cytomegalovirus infection. *Immunity* 50, 1391–1400.e4. <https://doi.org/10.1016/j.immuni.2019.04.015>.
33. Buchholz, V.R., Flossdorf, M., Hensel, I., Kretschmer, L., Weissbrich, B., Gráf, P., Verschoor, A., Schiemann, M., Höfer, T., and Busch, D.H. (2013). Disparate individual fates compose robust CD8+ T cell immunity. *Science* 340, 630–635. <https://doi.org/10.1126/science.1235454>.
34. Nauerth, M., Stemberger, C., Mohr, F., Weißbrich, B., Schiemann, M., Germeroth, L., and Busch, D.H. (2016). Flow cytometry-based TCR-ligand Koff-rate assay for fast avidity screening of even very small antigen-specific T cell populations ex vivo. *Cytometry A* 89, 816–825. <https://doi.org/10.1002/cyto.a.22933>.
35. Jutz, S., Leitner, J., Schmetterer, K., Doel-Perez, I., Majdic, O., Grabmeier-Pfistershamer, K., Paster, W., Huppa, J.B., and Steinberger, P. (2016). Assessment of costimulation and coinhibition in a triple parameter T cell reporter line: simultaneous measurement of NF- $\kappa$ B, NFAT and AP-1. *J. Immunol. Methods* 430, 10–20. <https://doi.org/10.1016/j.jim.2016.01.007>.
36. Sibener, L.V., Fernandes, R.A., Kolawole, E.M., Carbone, C.B., Liu, F., McAfee, D., Birnbaum, M.E., Yang, X., Su, L.F., Yu, W., et al. (2018). Isolation of a structural mechanism for uncoupling T cell receptor signaling from peptide-MHC binding. *Cell* 174, 672–687.e27. <https://doi.org/10.1016/j.cell.2018.06.017>.
37. Purcarea, A., Jarosch, S., Barton, J., Grassmann, S., Pachmayr, L., D'Ippolito, E., Hammel, M., Hochholzer, A., Wagner, K.I., van den Berg, J.H., et al. (2022). Signatures of recent activation identify a circulating T cell compartment containing tumor-specific antigen receptors with high avidity. *Sci. Immunol.* 7, eabm2077. <https://doi.org/10.1126/sciimmunol.abm2077>.
38. Fremont, D.H., Stura, E.A., Matsumura, M., Peterson, P.A., and Wilson, I.A. (1995). Crystal structure of an H-2Kb-ovalbumin peptide complex reveals the interplay of primary and secondary anchor positions in the major histocompatibility complex binding groove. *Proc. Natl. Acad. Sci. USA* 92, 2479–2483. <https://doi.org/10.1073/pnas.92.7.2479>.
39. Bentzen, A.K., Such, L., Jensen, K.K., Marquard, A.M., Jessen, L.E., Miller, N.J., Church, C.D., Lyngaa, R., Koelle, D.M., Becker, J.C., et al. (2018). T cell receptor fingerprinting enables in-depth characterization of the interactions governing recognition of peptide-MHC complexes. *Nat. Biotechnol.* <https://doi.org/10.1038/nbt.4303>.
40. Quinn, K.M., Zaloumis, S.G., Cukalac, T., Kan, W.T., Sng, X.Y.X., Mirams, M., Watson, K.A., McCaw, J.M., Doherty, P.C., Thomas, P.G., et al. (2016). Heightened self-reactivity associated with selective survival, but not expansion, of naïve virus-specific CD8+ T cells in aged mice. *Proc. Natl. Acad. Sci. USA* 113, 1333–1338. <https://doi.org/10.1073/pnas.1525167113>.
41. Kedzierska, K., Day, E.B., Pi, J., Heard, S.B., Doherty, P.C., Turner, S.J., and Perlman, S. (2006). Quantification of repertoire diversity of influenza-specific epitopes with predominant public or private TCR usage. *J. Immunol.* 177, 6705–6712. <https://doi.org/10.4049/jimmunol.177.10.6705>.
42. Enouz, S., Carrié, L., Merkler, D., Bevan, M.J., and Zehn, D. (2012). Autoreactive T cells bypass negative selection and respond to self-antigen stimulation during infection. *J. Exp. Med.* 209, 1769–1779. <https://doi.org/10.1084/jem.20120905>.
43. Meyer-Olson, D., Shoukry, N.H., Brady, K.W., Kim, H., Olson, D.P., Hartman, K., Shintani, A.K., Walker, C.M., and Kalams, S.A. (2004). Limited T cell receptor diversity of HCV-specific T cell responses is associated with CTL escape. *J. Exp. Med.* 200, 307–319. <https://doi.org/10.1084/jem.20040638>.
44. Oberle, S.G., Hanna-El-Daher, L., Chennupati, V., Enouz, S., Scherer, S., Prlic, M., and Zehn, D. (2016). A minimum epitope overlap between infections strongly narrows the emerging T cell repertoire. *Cell Rep.* 17, 627–635. <https://doi.org/10.1016/j.celrep.2016.09.072>.
45. Graef, P., Buchholz, V.R., Stemberger, C., Flossdorf, M., Henkel, L., Schiemann, M., Drexler, I., Höfer, T., Riddell, S.R., and Busch, D.H. (2014). Serial transfer of single-cell-derived immunocompetence reveals stemness of CD8(+) central memory T cells. *Immunity* 41, 116–126. <https://doi.org/10.1016/j.immuni.2014.05.018>.
46. Sung, J.H., Zhang, H., Moseman, E.A., Alvarez, D., Iannaccone, M., Henrickson, S.E., de La Torre, J.C., Groom, J.R., Luster, A.D., and von Andrian, U.H. (2012). Chemokine guidance of central memory T cells is critical for antiviral recall responses in lymph nodes. *Cell* 150, 1249–1263. <https://doi.org/10.1016/j.cell.2012.08.015>.
47. Pircher, H., Moskophidis, D., Rohrer, U., Bürki, K., Hengartner, H., and Zinkernagel, R.M. (1990). Viral escape by selection of cytotoxic T cell-resistant virus variants in vivo. *Nature* 346, 629–633. <https://doi.org/10.1038/346629a0>.
48. Haanen, J.B., Wolkers, M.C., Kruisbeek, A.M., and Schumacher, T.N. (1999). Selective expansion of cross-reactive CD8(+) memory T cells by viral variants. *J. Exp. Med.* 190, 1319–1328. <https://doi.org/10.1084/jem.190.9.1319>.
49. Caserta, S., Kleczkowska, J., Mondino, A., and Zamoyska, R. (2010). Reduced functional avidity promotes central and effector memory CD4 T cell responses to tumor-associated antigens. *J. Immunol.* 185, 6545–6554. <https://doi.org/10.4049/jimmunol.1001867>.
50. Zhong, S., Malecek, K., Johnson, L.A., Yu, Z., Vega-Saenz de Miera, E., Darvishian, F., McGary, K., Huang, K., Boyer, J., Corse, E., et al. (2013). T-cell receptor affinity and avidity defines antitumor response and autoimmunity in T-cell immunotherapy. *Proc. Natl. Acad. Sci. USA* 110, 6973–6978. <https://doi.org/10.1073/pnas.1221609110>.
51. Allard, M., Couturaud, B., Carretero-Iglesia, L., Duong, M.N., Schmidt, J., Monnot, G.C., Romero, P., Speiser, D.E., Hebeisen, M., and Rufer, N. (2017). TCR-ligand dissociation rate is a robust and stable biomarker of CD8+ T cell potency. *JCI Insight* 2. <https://doi.org/10.1172/jci.insight.92570>.
52. Alexander-Miller, M.A., Leggatt, G.R., and Berzofsky, J.A. (1996). Selective expansion of high- or low-avidity cytotoxic T lymphocytes and efficacy for adoptive immunotherapy. *Proc. Natl. Acad. Sci. USA* 93, 4102–4107. <https://doi.org/10.1073/pnas.93.9.4102>.
53. Foley, M.H., Forcier, T., McAndrew, E., Gonzalez, M., Chen, H., Juelg, B., Walker, B.D., and Irvine, D.J. (2014). High avidity CD8+ T cells efficiently eliminate motile HIV-infected targets and execute a locally focused program of anti-viral function. *PLoS One* 9, e87873. <https://doi.org/10.1371/journal.pone.0087873>.
54. Keane, N.M., Roberts, S.G., Almeida, C.A., Krishnan, T., Chopra, A., Demaine, E., Laird, R., Tschochner, M., Carlson, J.M., Mallal, S., et al. (2012). High-avidity, high-IFN $\gamma$ -producing CD8 T-cell responses following

- immune selection during HIV-1 infection. *Immunol. Cell Biol.* 90, 224–234. <https://doi.org/10.1038/icb.2011.34>.
55. Chung, B., Stuge, T.B., Murad, J.P., Beilhack, G., Andersen, E., Armstrong, B.D., Weber, J.S., and Lee, P.P. (2014). Antigen-specific inhibition of high-avidity T cell target lysis by low-avidity T cells via trogocytosis. *Cell Rep.* 8, 871–882. <https://doi.org/10.1016/j.celrep.2014.06.052>.
56. Ioannidou, K., Randin, O., Semiletov, A., Maby-El Hajjami, H., Baumgaertner, P., Vanhecke, D., and Speiser, D.E. (2019). Low avidity T cells do not hinder high avidity T cell responses against melanoma. *Front. Immunol.* 10, 2115. <https://doi.org/10.3389/fimmu.2019.02115>.
57. Jenkins, M.R., Webby, R., Doherty, P.C., and Turner, S.J. (2006). Addition of a prominent epitope affects influenza A virus-specific CD8+ T cell immunodominance hierarchies when antigen is limiting. *J. Immunol.* 177, 2917–2925. Baltimore, Md. <https://doi.org/10.4049/jimmunol.177.5.2917>.
58. Spear, T.T., Riley, T.P., Lyons, G.E., Callender, G.G., Roszkowski, J.J., Wang, Y., Simms, P.E., Scurti, G.M., Foley, K.C., Murray, D.C., et al. (2016). Hepatitis C virus-cross-reactive TCR gene-modified T cells: a model for immunotherapy against diseases with genomic instability. *J. Leukoc. Biol.* 100, 545–557. <https://doi.org/10.1189/jlb.2A1215-561R>.
59. Muschawechk, A., Buchholz, V.R., Fellenzer, A., Hessel, C., König, P.-A., Tao, S., Tao, R., Heikenwälder, M., Busch, D.H., Korn, T., et al. (2016). Antigen-dependent competition shapes the local repertoire of tissue-resident memory CD8+ T cells. *The Journal of experimental medicine* 213, 3075–3086. <https://doi.org/10.1084/jem.20160888>.
60. Wolf, F.A., Angerer, P., and Theis, F.J. (2018). SCANPY: large-scale single-cell gene expression data analysis. *Genome Biol.* 19, 15. <https://doi.org/10.1186/s13059-017-1382-0>.
61. Sturm, G., Szabo, T., Fotakis, G., Haider, M., Rieder, D., Trajanoski, Z., and Finotello, F. (2020). Scirpy: a Scanpy extension for analyzing single-cell T-cell receptor-sequencing data. *Bioinformatics Oxf. Engl.* 36, 4817–4818. <https://doi.org/10.1093/bioinformatics/btaa611>.
62. Mayer-Blackwell, K., Fiore-Gartland, A., and Thomas, P.G. (2022). Flexible distance-based TCR analysis in python with tcrdist3. *Methods Mol. Biol.* 2574, 309–366. [https://doi.org/10.1007/978-1-0716-2712-9\\_16](https://doi.org/10.1007/978-1-0716-2712-9_16).
63. Hunter, J.D. (2007). Matplotlib: A 2D Graphics Environment. *Comput. Sci. Eng.* 9, 90–95. <https://doi.org/10.1109/MCSE.2007.55>.
64. Waskom, M. (2021). seaborn: statistical data visualization. *JOSS* 6, 3021. <https://doi.org/10.21105/joss.03021>.
65. Virshup, I., Rybakov, S., Theis, F.J., Angerer, P., and Wolf, F.A. (2021). anndata: Annotated data. bioRxiv. <https://doi.org/10.1101/2021.12.16.473007>.
66. Busch, D.H., Pilip, I.M., Vijh, S., and Pamer, E.G. (1998). Coordinate regulation of complex T cell populations responding to bacterial infection. *Immunity* 8, 353–362. [https://doi.org/10.1016/S1074-7613\(00\)80540-3](https://doi.org/10.1016/S1074-7613(00)80540-3).
67. Pope, C., Kim, S.K., Marzo, A., Masopust, D., Williams, K., Jiang, J., Shen, H., and Lefrançois, L. (2001). Organ-specific regulation of the CD8 T cell response to *Listeria monocytogenes* infection. *J. Immunol.* 166, 3402–3409. Baltimore, Md. <https://doi.org/10.4049/jimmunol.166.5.3402>.
68. Dössinger, G., Bunse, M., Bet, J., Albrecht, J., Paszkiewicz, P.J., Weißbrich, B., Schiedewitz, I., Henkel, L., Schiemann, M., Neuenhahn, M., et al. (2013). MHC multimer-guided and cell culture-independent isolation of functional T cell receptors from single cells facilitates TCR identification for immunotherapy. *PLoS One* 8, e61384. <https://doi.org/10.1371/journal.pone.0061384>.
69. Nauerth, M., Weißbrich, B., Knall, R., Franz, T., Dössinger, G., Bet, J., Paszkiewicz, P.J., Pfeifer, L., Bunse, M., Uckert, W., et al. (2013). TCR-ligand koff rate correlates with the protective capacity of antigen-specific CD8+ T cells for adoptive transfer. *Sci. Transl. Med.* 5, 192ra87. <https://doi.org/10.1126/scitranslmed.3005958>.
70. Luecken, M.D., and Theis, F.J. (2019). Current best practices in single-cell RNA-seq analysis: a tutorial. *Mol. Syst. Biol.* 15, e8746. <https://doi.org/10.1522/msb.20188746>.
71. Polański, K., Young, M.D., Miao, Z., Meyer, K.B., Teichmann, S.A., and Park, J.E. (2020). BBKNN: fast batch alignment of single cell transcriptomes. *Bioinformatics Oxf. Engl.* 36, 964–965. <https://doi.org/10.1093/bioinformatics/btz625>.
72. Bernstein, N.J., Fong, N.L., Lam, I., Roy, M.A., Hendrickson, D.G., and Kelley, D.R. (2020). Solo: doublet identification in single-cell RNA-seq via semi-supervised deep learning. *Cell Syst.* 11, 95–101.e5. <https://doi.org/10.1016/j.cels.2020.05.010>.
73. Schattgen, S.A., Guion, K., Crawford, J.C., Souquette, A., Barrio, A.M., Stubbington, M.J.T., Thomas, P.G., and Bradley, P. (2022). Integrating T cell receptor sequences and transcriptional profiles by clonotype neighbor graph analysis (CoNGA). *Nat. Biotechnol.* 40, 54–63. <https://doi.org/10.1038/s41587-021-00989-2>.
74. Fuchs, Y.F., Sharma, V., Eugster, A., Kraus, G., Morgenstern, R., Dahl, A., Reinhardt, S., Petzold, A., Lindner, A., Löbel, D., and Bonifacio, E. (2019). Gene expression-based identification of antigen-responsive CD8+ T cells on a single-cell level. *Front. Immunol.* 10, 2568. <https://doi.org/10.3389/fimmu.2019.02568>.
75. Kozak, M. (1987). An analysis of 5'-noncoding sequences from 699 vertebrate messenger RNAs. *Nucleic Acids Res.* 15, 8125–8148. <https://doi.org/10.1093/nar/15.20.8125>.

## STAR★METHODS

## KEY RESOURCES TABLE

REAGENT or RESOURCE	SOURCE	IDENTIFIER
<b>Antibodies</b>		
aCD45.1 FITC	BioLegend	110706, RRID: AB_313495
aCD45.1 PE	BioLegend	110708, RRID: AB_313496
aCD45.1 PE-Cy7	BioLegend	110730, RRID: AB_1134168
aCD45.1 PB450	BioLegend	110722, RRID: AB_492867
aCD45.1 BV785	BioLegend	110743, RRID: AB_2563379
aCD90.1 APC	Life Technologies	17-0900-82, RRID: AB_469420
aCD90.1 eF450	Life Technologies	48-0900-82, RRID: AB_1272254
aCD4 PE-Dazzle 594	BioLegend	100565, RRID: AB_2563684
aCD19 PE-Dazzle 594	BioLegend	115553, RRID: AB_2564000
aCD8a Pacific Blue	BioLegend	100725, RRID: AB_493425
aCD8a Pacific Blue	Life Technologies	MCD0828, RRID: AB_10372364
aCD8a BV785	BioLegend	100750, RRID: AB_2562610
aCD8a PE	Life Technologies	MCD0804, RRID: AB_10373415
aCD8a Pacific Orange	Life Technologies	MCD0830, RRID: AB_10376311
aCD62L APC	BioLegend	104412, RRID: AB_313099
aCD62L BV785	BioLegend	104440, RRID: AB_2629685
aCD27PE-Cy7	Life Technologies	25-0271-82, RRID: AB_1724035
aCD44 FITC	BioLegend	103022, RRID: AB_493685
aCD44 PE	BioLegend	103007, RRID: AB_312958
aCD44 AF700	BioLegend	103025, RRID: AB_493712
aPD-1 PE	Life Technologies	12-9985-81, RRID: AB_466294
aCD69 FITC	BioLegend	104505, RRID: AB_313109
aCD69 PC7	BioLegend	104511, RRID: AB_313109
aCD3 PE	BioLegend	100308, RRID: AB_312673
aCD3 PE-Dazzle 594	BioLegend	100348, RRID: AB_2564028
aCD3 purified	BioLegend	100302, RRID: AB_312666
aCD28 purified	BD Biosciences	553295, RRID: AB_394764
aSca1 PE	BioLegend	108107, RRID: AB_313344
aTCR β-chain APC	BioLegend	109212, RRID: AB_313434
aCD16/32 purified (Fc Block)	BioLegend	101301, RRID: AB_312801
TotalSeq™-C0301 anti-mouse Hashtag 1	BioLegend	155861, RRID: AB_2800693
TotalSeq™-C0302 anti-mouse Hashtag 2	BioLegend	155863, RRID: AB_2800694
TotalSeq™-C0303 anti-mouse Hashtag 3	BioLegend	155865, RRID: AB_2800695
TotalSeq™-C0304 anti-mouse Hashtag 4	BioLegend	155867, RRID: AB_2800696
TotalSeq™-C0305 anti-mouse Hashtag 5	BioLegend	155869, RRID: AB_2800697
TotalSeq™-C0306 anti-mouse Hashtag 6	BioLegend	155871, RRID: AB_2819910
TotalSeq™-C0307 anti-mouse Hashtag 7	BioLegend	155873, RRID: AB_2819911
TotalSeq™-C0308 anti-mouse Hashtag 8	BioLegend	155875, RRID: AB_2819912
TotalSeq™-C0309 anti-mouse Hashtag 9	BioLegend	155877, RRID: AB_2819913
TotalSeq™-C0310 anti-mouse Hashtag 10	BioLegend	155879, RRID: AB_2819914
aCD8 APC (human)	eBioscience	25-0086-42, RRID: AB_2637437
<b>Bacterial and virus strains</b>		
Listeria monocytogenes-N4/Y3/T4	Zehn et al. <sup>22</sup>	N/A
MVA-PH5-OVA	Muschawecckh et al. <sup>59</sup>	N/A

(Continued on next page)

***Continued***

REAGENT or RESOURCE	SOURCE	IDENTIFIER
<b>Chemicals, peptides, and recombinant proteins</b>		
Propidium Iodide (PI)	Life Technologies	Cat#P1304MP
Recombinant murine IL-3	PeproTech	Cat#213-13
Recombinant murine IL-6	PeproTech	Cat#216-16
Recombinant murine SCF	PeproTech	Cat#250-03
Recombinant human IL-2	PeproTech	Cat#200-07
RetroNectin®	Takara Bio Europe	Cat#T100B
Phorbol 12-myristate 13-acetate (PMA)	Sigma Aldrich	Cat#16561-29-8
Ionomycin	Sigma Aldrich	Cat#56092-81-0
dNTPs	Roche	Cat#11969064001
DTT	Sigma-Aldrich	Cat#3483-12-3
Igepal CA-630	Sigma-Aldrich	Cat#I8896-50ML
RNAsin Plus	Promega	Cat#N2611
dNTP transferase	Promega	Cat#M828A
Affinityscript reverse transcriptase	Agilent	Cat#600107
Exonuclease I	Teruo Fisher Scientific	Cat#EN0581
RPMI 1640 Gibco	Sigma Aldrich	Cat# R0883
DMEM	Life Technologies	Cat# 10938025
Fetal calf serum	Biochrom	N/A
Gentamicin	Life Technologies	Cat# 15750-037
L-Glutamine	Sigma-Aldrich	Cat# G8540-100G
Penicillin/Streptomycin	Life Technologies	Cat# 10378016
HEPES	Life Technologies	Cat# 15630056
Retronectin	TaKaRa	Cat# T100B
DNA LoBind tubes	Sigma-Aldrich	Cat# EP0030108051, EP0030108078, EP0030124359
RPT filter tips	Starlab	Cat# S1183-1710, SS1180-8710, S1182-1730
<b>Critical commercial assays</b>		
High sensitivity DNA Kit	Agilent	#5067-4626
Qubit dsDNA hs assay kit	Life Technologies	#Q32851
<b>Experimental models: Cell lines</b>		
Platinum E cells	Cell Biolabs	Cat#RV-101
Jurkat triple parameter reporter cells	In house	N/A
RD114	In house	N/A
<b>Experimental models: Organisms/strains</b>		
C57Bl/6JOlαHsd	Envigo	Stock number: 057, RRID: IMSR_ENV:HSD-057
C57BL/6-Tg(TcrαTcrβ)1100Mjb/J	The Jackson Laboratory	Stock number: 003831, RRID: IMSR_JAX:003831
B6.129S2-Tcr <sup>tm1Mom</sup> /J	The Jackson Laboratory	Stock number: 002116, RRID: IMSR_JAX:002116
B6.129S7-Rag1tm1Mom/J	The Jackson Laboratory	Stock number: 002216, RRID:IMSR_JAX:002216
<b>Oligonucleotides</b>		
Primer sequences for single cell PCR are listed in <b>Table S4</b>		N/A
<b>Recombinant DNA</b>		
MP71 vector for retrovirus generation in Plat E and RD114 cells	Addgene	#108214
<b>Software and algorithms</b>		
FloJo V10	FlowJo LLC	<a href="https://www.flowjo.com/">https://www.flowjo.com/</a>
Prism 9	Graphpad	<a href="https://www.graphpad.com">https://www.graphpad.com</a>
Microsoft Excel	Microsoft	N/A
Python 3.8.5	Python Software Foundation	N/A

(Continued on next page)

**Continued**

REAGENT or RESOURCE	SOURCE	IDENTIFIER
Scanpy 1.8.2	Wolf et al. <sup>60</sup>	<a href="https://scanpy.readthedocs.io/en/stable/">https://scanpy.readthedocs.io/en/stable/</a>
Scirpy 0.10.1	Sturm et al. <sup>61</sup>	<a href="https://icbi-lab.github.io/scirpy/">https://icbi-lab.github.io/scirpy/</a>
Tcrdist3 0.2.2	Mayer-Blackwell et al. <sup>62</sup>	<a href="https://tcrdist3.readthedocs.io/en/latest/">https://tcrdist3.readthedocs.io/en/latest/</a>
Matplotlib 3.4.2	Hunter <sup>63</sup>	<a href="https://matplotlib.org/">https://matplotlib.org/</a>
Seaborn 0.11.1	Waskom <sup>64</sup>	<a href="https://seaborn.pydata.org/">https://seaborn.pydata.org/</a>
Anndata 0.7.6	Virshup et al. <sup>65</sup>	<a href="https://anndata.readthedocs.io/en/latest/">https://anndata.readthedocs.io/en/latest/</a>
Cell Ranger 5.0.0/6.0.2	10X genomics	<a href="https://support.10xgenomics.com/single-cell-gene-expression/software/pipelines/latest/installation">https://support.10xgenomics.com/single-cell-gene-expression/software/pipelines/latest/installation</a>
Affinity Designer 1.9	Serif	<a href="https://affinity.serif.com/">https://affinity.serif.com/</a>
<b>Other</b>		
H2-Kb/m $\beta$ 2m/Ova 257-264	Busch et al. <sup>66</sup>	N/A
Streptavidin-PE/APC/BV421		
H2-Kb/m $\beta$ 2m/M38 316-323	Busch et al. <sup>66</sup>	N/A
Streptavidin-APC		

**RESOURCE AVAILABILITY****Lead contact**

Further information and requests for resources and reagents should be directed to and will be managed by the lead contact, Dirk H. Busch ([dirk.busch@tum.de](mailto:dirk.busch@tum.de)).

**Materials availability**

This study did not generate new unique reagents.

**Data and code availability**

All data and [supplemental information](#) generated or analyzed during this study are included in this article. This paper does not report original code. Any additional information and notebooks containing all steps of data processing and analysis of single-cell RNA sequencing reported in this paper are available on GitHub ([https://github.com/AdrianStraub/2022\\_Straub\\_et\\_al\\_scRNASeq\\_Recruitment\\_of\\_epitope\\_specific\\_T\\_cells](https://github.com/AdrianStraub/2022_Straub_et_al_scRNASeq_Recruitment_of_epitope_specific_T_cells)). Any additional information or raw data are available from the [lead contact](#) upon reasonable request.

**EXPERIMENTAL MODEL AND SUBJECT DETAILS****Mice**

C57BL/6JOlA-Hsd (females, 6–10 weeks) were purchased from Envigo. 6–24 weeks old female SIINFEKL peptide-specific TCR transgenic OT-I (C57BL/6-Tg(TcraTcrb)1100Mjb/J), 6–24 weeks old female and male TCRA<sup>-/-</sup> (B6.129S2-Tcra tm1Mom/J) and Rag<sup>-(B</sup> mice (B6.129S7-Rag1tm1Mom/J) were originally obtained from The Jackson Laboratory and bred under specific pathogen-free conditions at our mouse facility at the Technical University of Munich. Different congenic marker backgrounds of CD45.1/2 and CD90.1/2 were derived from in-house breeding.<sup>33</sup> All animal experiments were approved by the district government of upper Bavaria (Department 5 – Environment, Health and Consumer Protection; vote 55.2-2532.Vet\_02-21-155).

**Cell lines**

Platinum E and RD114 cell lines were grown in cDMEM, supplemented with 10% FCS, 0.025% L-Glutamine, 0.1% HEPES, 0.001% gentamycin and 0.002% streptomycin). JTPR cell lines and primary T cells were cultured in RPMI 1640 supplemented with 10% FCS, 0.025% L-glutamine, 0.1% HEPES, 0.001% gentamycin and 0.002% streptomycin. Primary T-cell culture was additionally supplemented with 25 IU mL<sup>-1</sup> IL-2. All cells were grown in a 37°C humidified, 5% CO<sub>2</sub> incubator. JTPRs were originally obtained from Peter Steinberger (Medizinische Universität Wien).

**METHOD DETAILS****Infections**

Primary infections: Mice were infected i.v. with 5000 colony-forming units (CFU) of recombinant *Listeria monocytogenes* expressing Ovalbumin<sup>67</sup> or i.p. with MVA-PH5-OVA (1×10<sup>7</sup> plaque-forming units (pfu)).

Secondary infections: Mice were infected i.v. with 200.000 (data related to [Figure 6A](#)) or 20.000 (data related to [Figure 6F](#)) CFU of recombinant Listeria monocytogenes expressing Ovalbumin with either of the epitopes SIINFEKL, SIYNFEKL or SIITFEKL as indicated in figure descriptions.

### Generation of retroviruses

For retrovirus production, Platinum-E or RD114 packaging cells were transfected with the retroviral vectors (mp71, a kind gift from W. Uckert, added as Addgene plasmid backbone #108214) encoding for the respective SIINFEKL-reactive TCRs via calcium phosphate precipitation. The supernatant of the Platinum-E or RD114 cells was collected at 48 and 72 h after transfection and purified from remaining cells by centrifugation at 1,500 r.p.m. at 4 °C for 7 min. The supernatant was stored at 4 °C and used within 4 weeks after collection. Retroviral fluorescent barcodes were produced in the same manner.

### Generation of T cell retrogenic mice

Bone marrow was collected from the tibia and femur of 8–20-week-old donor mice (congenic matrix, Rag-1<sup>-/-</sup>). After red blood cell lysis, the cells were brought into single-cell suspension and stained with anti-mouse Ly6A/E (Sca-1) and anti-mouse CD3 and CD19 antibodies. Propidium iodide (PI) was used for live/dead discrimination. Sorted Sca-1-positive, CD3 and CD19 negative cells were incubated at 37 °C in cDMEM, supplemented with 2 ng ml<sup>-1</sup> murine IL-3, 50 ng ml<sup>-1</sup> murine IL-6 and 50 ng ml<sup>-1</sup> murine stem cell factor (mSCF), for 4 days in a tissue-culture-treated 48-well plate (250,000–300,000 cells per 400 µl). Retroviral transduction of the expanded stem cells with the respective TCR and fluorescent barcode was achieved by spinoculation. In brief, 400 µl of the combined Platinum-E supernatants were centrifuged at 3,000g at 32 °C for 2 h in a tissue-culture-untreated 48-well plate coated with RetroNectin according to the manufacturer's instructions. Afterwards, the supernatant was discarded, and stem cells were added in stimulation medium (2 ng ml<sup>-1</sup> mIL-3, 50 ng ml<sup>-1</sup> mIL-6 and 50 ng ml<sup>-1</sup> mSCF) in a final concentration of 300,000 cells per 400 µl per well. Cells were then spinoculated at 800g at 32 °C for 1.5 h. After 2 days in culture the transduced stem cells were suspended in FCS at 500,000–1,000,000 cells per 200 µl and injected intravenously into irradiated C57BL/6 recipient mice (two times 4.5 Gy, with a resting period of 4 h).

### Flow cytometry

Spleens and/or lymph nodes were collected and mashed through a 70-µm cell strainer to generate a single-cell suspension. Spleenocytes and peripheral blood mononuclear cells, following red blood cell lysis, were stained with the respective antibody panel for 25 min at 4 °C in the dark (Multimer staining described separately). After washing with FACS buffer (PBS with 0.5% BSA and 2 mM EDTA), the cells were stained with PI for 5 min and washed again. Data were collected by flow cytometry on a Cytoflex S or Cytoflex LX flow cytometer (Beckman Coulter). For analysis, FlowJo software (FlowJo LLC) was used. See [Figures S4](#) and [S5](#) for representative gating scheme of flow cytometry experiments.

### Peptide-MHC (pMHC) multimer staining

Biotinylated pMHC molecules for the generation of pMHC multimers were refolded according to the protocol as previously described.<sup>66</sup> 0,4 µg of biotinylated pMHC I molecule, 0,5 µg of Streptavidin-PE, Streptavidin-APC or Streptavidin-BV421 and 50 µl of FACS buffer for every 5×10<sup>6</sup> cells, were preincubated for at least 30 min for multimerization. Cells were then incubated with the multimer mix for 40 min. 20 min before the end of the staining period antibodies for the staining of surface antigens were added. PI for live/dead staining was added 5 min before the end of the staining period.

### Speed enrichment and single-cell sorting

Spleens, inguinal, axillary and mesenteric lymph nodes were harvested from naïve WT C57BL/6 mice. Blood from CD45.1<sup>+/+</sup> Rag1<sup>-/-</sup> OT-I transgenic mice was collected. Whole WT samples and OT-I T cells were stained for Fc-block (1:400) followed by pMHC-multimer staining (Streptavidin-APC) as described. 1 × 10<sup>4</sup> Multimer+ OT-I T cells were sorted (MoFlo legacy; Beckman Coulter) into WT samples. ‘Speed enrichment’ for APC positive cells was subsequently performed on whole WT samples. In short: A fluorescent trigger was set on a MoFlo Astrios EQ (Beckman Coulter) on the APC (multimer) fluorescence channel. The trigger change from regular forward scatter to a depicted threshold of fluorescence positive cells blinds the machine to any particle negative for the fluorescent signal. This leads to a drastic decrease in detected events and allows for rapid sorting of large cell quantities. APC<sup>+</sup> cells were sorted into a 15 ml Falcon in FCS. The cells were washed and stained for a second pMHC multimer (Streptavidin BV-421), followed by staining against surface antigens (CD4, CD19, CD8, CD44, CD62L, CD45.1) as described. Single naïve CD8 T cells were sorted for CD4<sup>-</sup> CD19<sup>-</sup> CD45.1<sup>-</sup> CD8<sup>+</sup> CD44<sup>lo</sup> CD62L<sup>hi</sup> Ova-multimer-APC<sup>+</sup> Ova-multimer-BV421<sup>+</sup> into FCS of an anti-CD3, anti-CD28 coated 384well plate. Single cells were expanded for 7 to 10 days and processed for single-cell PCR to identify TCR sequences.

### Single-cell PCR

Single-cell PCR of the TCR (TCR SCAN) was adapted from the TCR SCAN platform as previously described.<sup>68</sup> Single clone expanded cells were resuspended in 2.0 µl of 50 mM Tris-HCl (pH 8.3), 75 mM KCl, 3 mM MgCl<sub>2</sub>, 1,6 mM dNTPs, 10 mM DTT, 0.1 mg/ml BSA, 0.1 mg/ml tRNA, 0.25% Igepal CA-630, 0.8 U/µl RNAsin Plus, 1 µM reverse transcription primers ([Table S4](#)) and 0.05 rxn/ µl Affinity-script reverse transcriptase. Samples were covered with 10 µl of PCR oil. Reverse transcription was performed for 30 min at 51°C

followed by 20 min at 70°C on an AmpliSpeed PCR cycler. For primer exonuclease I digest, reaction volume was filled up to 2.5 µl with buffer including a final concentration of 1 U/µl Exonuclease I. Exonuclease-I digest was performed for 30 min at 37°C and enzyme was inactivated for 20 min at 70°C. Samples were transferred to a 96well plate and poly-guanine tailing was performed by adding 7 µl of 100 mM MgCl<sub>2</sub>, 10 mM DTT, 100 mM Tris (pH 7.5) and 20 mM dGTP and 0.75 U/µl terminal dNTP transferase. Tailing reaction was performed for 45 min at 37°C and enzyme was inactivated for 15 min at 70°C. For anchor PCR 40 µl of 1X Herculase II reaction buffer, including 0.20 mM dNTPs, 3% formamide, 0.02 rxn/µl Herculase II DNA polymerase and 0.5 µM of each primer ([Table S4](#)) were added and covered with 20 µl of PCR oil. PCR was performed as follows: 94°C 3 min for initial denaturation followed by 24 cycles of 94°C for 30 s, 60°C for 30 s, 72°C for 45 s and 72°C for 5 min as final extension step. 1 µl of product was transferred to nested PCR amplification in separate reactions for α- and β- chain ([Table S4](#)). PCR conditions for nested PCR round I and II were identical to anchor PCR except for primers.

### Adoptive transfer and tracking of T cells

For adoptive transfer experiments TCR retrogenic donors with TCRs of different avidities for H-2K<sup>b</sup>/SIINFEKL on a unique congenic marker (CD45, CD90) or fluorescent barcode (GFP, YFP, BFP, CFP, Ametrine) background were used. Blood or spleens from retrogenic mice were stained following red blood cell lysis with antibodies directed against CD8, CD44 and CD45.1 or CD90.1 with PI staining for live/dead discrimination. Naïve T cells (living, CD8<sup>+</sup>, CD44<sup>lo</sup>, congenic<sup>+</sup>) were sorted (MoFlo legacy, MoFlo Astrios EQ; Beckman Coulter) into a 96-well v-bottom plate containing a cell pellet of 400.000 C57BL/6 splenocytes (TCRα<sup>-/-</sup> splenocytes for TCRα<sup>-/-</sup> recipients) in FCS. Cells were injected i.p. into recipients. Peripheral blood of recipient mice was analyzed via flow cytometry at different timepoints after transfer. The unique congenic marker or fluorescent barcode allowed tracking of individual TCRs over time. Sequences of all reexpressed murine TCRs can be found in [Table S2](#).

### Flow-cytometry-based TCR-ligand $k_{off}$ -rate

$k_{off}$ -rate assays were performed as previously described.<sup>69</sup> In brief, reversible multimers were generated by adding 1 µg of the respective Alexa Fluor 488-conjugated pMHC I molecule (Strep-tagIII/mβ2m cys67), 0.75 µg of Strep-Tactin-APC and 50 µl of FACS buffer for every 5 × 10<sup>6</sup> cells, and incubated for at least 30 min. Splenocytes from TCR retrogenic donors were then incubated with the multimer mix for 45 min. At 20 min before the end of the staining period antibodies for the staining of surface antigens were added. PI for live/dead staining was added 5 min before the end of the staining period. Samples were transferred into precooled FACS tubes containing a total volume of 1 ml of FACS buffer and placed into a Peltier cooler (qtools GmbH) set to 5.5 °C. After 30 s acquisition, 1 ml of cold 2 mM d-biotin was added into the ongoing measurement. Dissociation kinetics were measured for at least 10 min. For analysis of  $k_{off}$ -rate data, fluorescence data of congenically marked antigen-reactive T cells were exported from FlowJo to PRISM (GraphPad Software). The  $t_{1/2}$  was determined by fitting a one-phase exponential decay curve.

### Antigen-specific activation of primary T cells

Spleens were isolated from naïve retrogenic donors. 1 × 10<sup>6</sup> splenocytes were separately incubated with different peptide concentrations (10<sup>-12</sup> M, 10<sup>-10</sup> M, 10<sup>-9</sup> M, 10<sup>-8</sup> M, 10<sup>-7</sup> M, 10<sup>-6</sup> M, 10<sup>-5</sup> M, 10<sup>-4</sup> M) of the SIINFEKL-peptide, SIYNFEKL-peptide (10<sup>-4</sup>M), SIITFEKL-peptide (10<sup>-4</sup>M), a negative (RP10<sup>+</sup> only) and a positive control (purified anti-CD3 0.5 µg ml<sup>-1</sup>, purified anti-CD28 0.25 µg ml<sup>-1</sup>). Samples were then incubated at 37 °C for 18 hours. Next Fc-block staining (1:400) and staining of surface antigens (CD8, CD19, CD45.1 or CD90.1, CD3, CD69) were performed. The maximal percentage of CD69<sup>+</sup> as well as CD3<sup>lo</sup> CD8<sup>+</sup> cells was normalized to 100%, and a nonlinear curve was fitted into the normalized data.

### In vivo L.m. OVA proliferation

Mice were injected with 50 or 500 naïve retrogenic T cells (i.p) for each TCR and infected with 5000 CFU *L.m.* OVA (i.v.). On day 8 after infection, spleens were harvested and processed as described. Fc-block staining (1:400) and staining of surface antigens (CD8, CD19, CD45.1 or CD90.1, CD44, CD62L, CD27) were performed. The same staining procedure was performed for blood sampling at different timepoints. Samples were subsequently analyzed by flow cytometry.

### Antigen-specific activation of human JTPR

Spleens were harvested for antigen presenting cells from naïve WT C57BL/6 mice and 1.2 × 10<sup>5</sup> splenocytes were loaded with different peptide concentrations (10<sup>-12</sup> M, 10<sup>-4</sup> M) of the SIINFEKL-peptide, SIYNFEKL-peptide (10<sup>-4</sup>M), SIITFEKL-peptide (10<sup>-4</sup>M), a negative (RP10<sup>+</sup> only) and a positive control (PMA 0.025 µg ml<sup>-1</sup>, Ionomycin 1.0 µg ml<sup>-1</sup>). 2.4 × 10<sup>4</sup> TCR transduced JTPR were added to each condition in parallel in separate stimulations. Samples were then incubated at 37 °C for 20 hours. The same JTPR were stained in a separate incubation for surface antigens (human CD8, murine TCR β-chain). The percentage of NFAT<sup>+</sup> (GFP reporter) JTPR after stimulation was assessed via flow cytometry and normalized according to the fraction of transgenic TCR expressing JTPR. Live/dead discrimination was performed with propidium iodide. Activation of TCR transgenic JTPR with the SIINFEKL-APL library was performed equally. JTPR of one TCR were incubated in parallel with APL-peptide (10<sup>-4</sup> M) pulsed splenocytes in separate stimulations alongside a negative (as described) and positive control (as described). A full list of the SIINFEKL-APL library can be found in [Table S3](#).

### Quantification of colony forming units (CFUs)

Spleens were collected and mashed through a 70- $\mu\text{m}$  cell strainer to generate a single-cell suspension. 50% of the spleens were used to determine CFUs. Whole livers were collected and used to determine CFUs. 50% of spleen and whole liver were separately collected in 2.5 ml total volume of sterile PBS and homogenized. 10-fold dilution series of the homogenates was performed in 0.1% Triton-X-100 in PBS ranging from undiluted (300 $\mu\text{l}$  total volume) to  $10^{-5}$ . 150 $\mu\text{l}$  of each diluted homogenate were spread onto a brain heart infusion (BHI) agar plate using a sterile spreader and transferred over night to a 37°C incubator. Mean number of colonies were determined across dilutions. Undiluted count contained 3% of total spleen and 6% of total liver, respectively. Whole organ count was calculated according to 10-fold dilution factor of counting plates and initial spleen (3%) and liver (6%) input.

### Antigen-specific activation for single-cell RNA sequencing

Splenocytes were isolated from *L.m.-N4* infected C57BL/6 donors. 1  $\times$  10 $^6$  splenocytes from each donor were separately incubated with 10 $^{-4}$ M SIINFEKL-peptide (dissolved in ddH<sub>2</sub>O) or left unstimulated (medium only). Samples were then incubated at 37 °C for 4 hours. TotalSeq™-C0301310 anti-mouse Hashtag antibodies targeting MHC class I and CD45 were stained following the manufacturer's instructions. Staining with fluorescent antibodies was performed in parallel. Splenocytes were stained for CD4, CD19, CD8, CD44 and either with or without H-2K<sup>b</sup>/SIINFEKL Streptavidin-APC. Individual donors were labelled with a unique TotalSeq™-C anti-mouse Hashtag antibody. 3500 cells were sorted per donor for CD4<sup>+</sup> CD19<sup>-</sup> CD8<sup>+</sup> CD44<sup>hi</sup>, if H-2K<sup>b</sup>/SIINFEKL was stained, cells were additionally sorted for multimer<sup>+</sup> or multimer<sup>-</sup>.

### Single-cell RNA sequencing

After cells have been sorted, they were centrifuged and the supernatant was carefully removed. Cells were resuspended in the Mastermix + 37.8  $\mu\text{l}$  of water before 70  $\mu\text{l}$  of the cell suspension were transferred to the chip. (Step 1.1 and 1.2 of the original protocol). After each step, the integrity of the pellet was checked under the microscope to ensure that all cells are loaded onto the chip. From here on, 10x experiments have been performed according to the manufacturer's protocol (Chromium next GEM Single Cell VDJ V1.1 with Feature Barcode, Rev D). QC has been performed with a High sensitivity DNA Kit on a Bioanalyzer 2100 as recommended in the protocol and libraries were quantified with the Qubit dsDNA hs assay kit. All steps have been performed using RPT filter tips and DNA LoBind tubes.

### scRNA-seq data analysis

References GRCh38-2020-A and vdj\_GRCh38\_alts\_ensembl-5.0.0 were used for Transcriptome and VDJ annotation (CellRanger 5.0.0 and CellRanger 6.0.2), respectively. Data preprocessing has been performed according to the current best practice in scRNA sequencing analysis.<sup>70</sup> Data analysis was performed with SCANPY V1.8.2<sup>60</sup> and Scirpy 0.10.1.<sup>61</sup> Briefly, cells with less than 200 genes as well as genes present in less than three cells were excluded. Counts were normalized per cell, logarithmized and the variance was scaled to unit variance and zero mean. The number of counts, percentage of mitochondrial genes and cell cycle score was regressed out before highly variable genes were identified and filtered. The data was batch corrected using batch-balanced k nearest neighbors (bbknn)<sup>71</sup> for individual experiments. DNA-Barcode demultiplexing was performed with HashSolo included in SCANPY.<sup>72</sup> TCR clustering was performed with TCRdist3<sup>62</sup> and CONGA.<sup>73</sup> Identified antigen-reactive clonotypes with minimum clonal expansion can be found in Table S1. The used 'activation' score encompassed expression of Trfrsf9, Ifng, Xcl1, Ccl3, Ccl4, Rgs16, Srm, Irf8, Nr4a1, Cd160, related to previously defined signatures of activated murine T cells.<sup>74</sup>

### Clonotype definition from single-cell RNA sequencing data

Clonotype analysis was performed using Scirpy.<sup>61</sup> Cells belonging to one clonotype were defined to have identical  $\alpha$  and  $\beta$  chain CDR3 nucleotide sequences. Only primary pairs of TRA/TRB chains were considered when multiple chains were detected.

### TCR DNA template design

DNA templates were designed *in silico* and synthesized by Twist Bioscience in a retroviral vector. DNA constructs had the following structure: Murine Kozac Sequence,<sup>75</sup> TCR  $\beta$  including mTRBC1, P2A, TCR  $\alpha$ , including mTRAC), cloned into the pMP71 vector (kindly provided by Wolfgang Uckert, Berlin). All TCR constructs for retroviral transduction are listed in Table S2.

### QUANTIFICATION AND STATISTICAL ANALYSES

Statistical analyses were performed using the GraphPad PRISM software. Statistical tests were used as indicated in the figure legends. Sample sizes for *in vivo* experiments were determined given estimated effect sizes based on preliminary experiments with a type I error of 0.05 and a type 2 error of 0.2.

**Supplemental information**

**Recruitment of epitope-specific T cell clones  
with a low-avidity threshold supports efficacy  
against mutational escape upon re-infection**

**Adrian Straub, Simon Grassmann, Sebastian Jarosch, Lena Richter, Philipp Hilgendorf, Monika Hammel, Karolin I. Wagner, Veit R. Buchholz, Kilian Schober, and Dirk H. Busch**

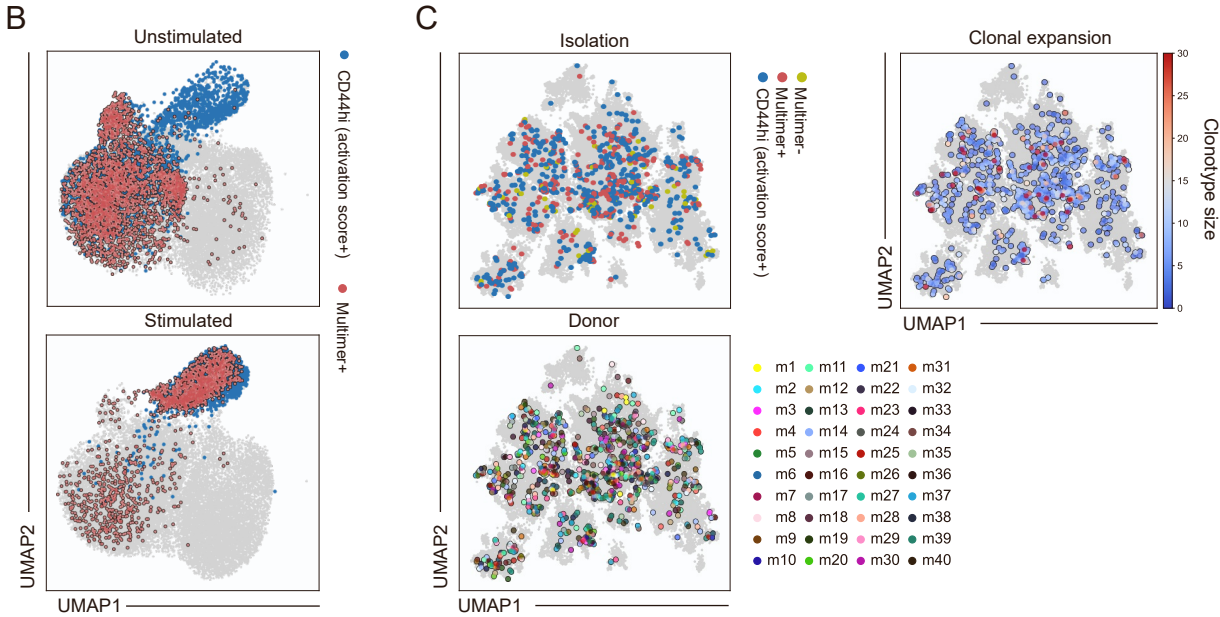
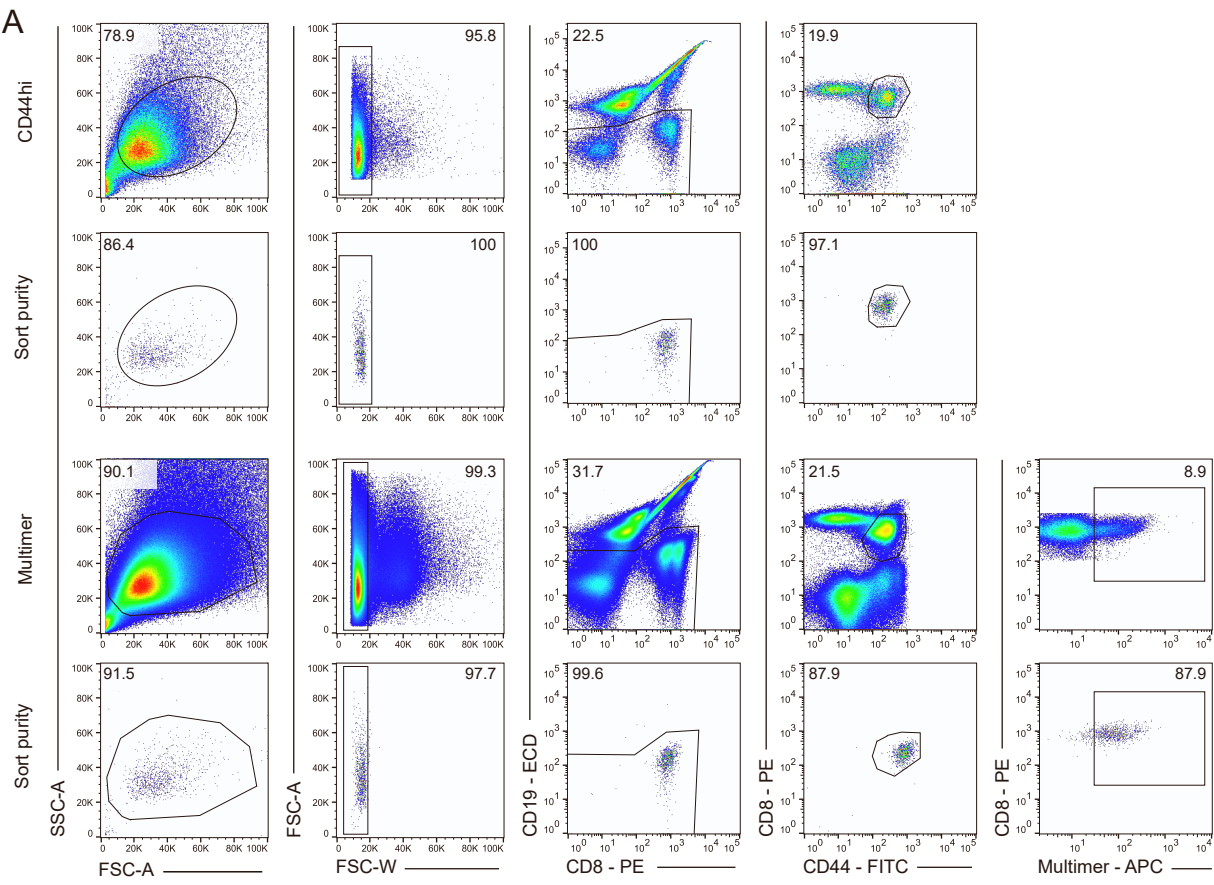


**Fig. S1. Sorting strategy and sort purity of activated T cells, related to Fig. 1.**

(A), Gating strategy for scRNA sequencing sort showing 2 exemplary sample sources (CD44<sup>hi</sup> and multimer+), as well as the respective purity control. Numbers indicate percentages. (B), UMAP of antigen-score (+) and multimer (+) cells in unstimulated state (top) and stimulated state bottom). (C), UMAP projection of the TCR sequence neighbor graph as produced by clonotype neighbour graph analysis (CoNGA)<sup>69</sup>, SIINFEKL-reactive clones are highlighted by isolation methods (top left), donor distribution (bottom left) and clonal expansion (top right).

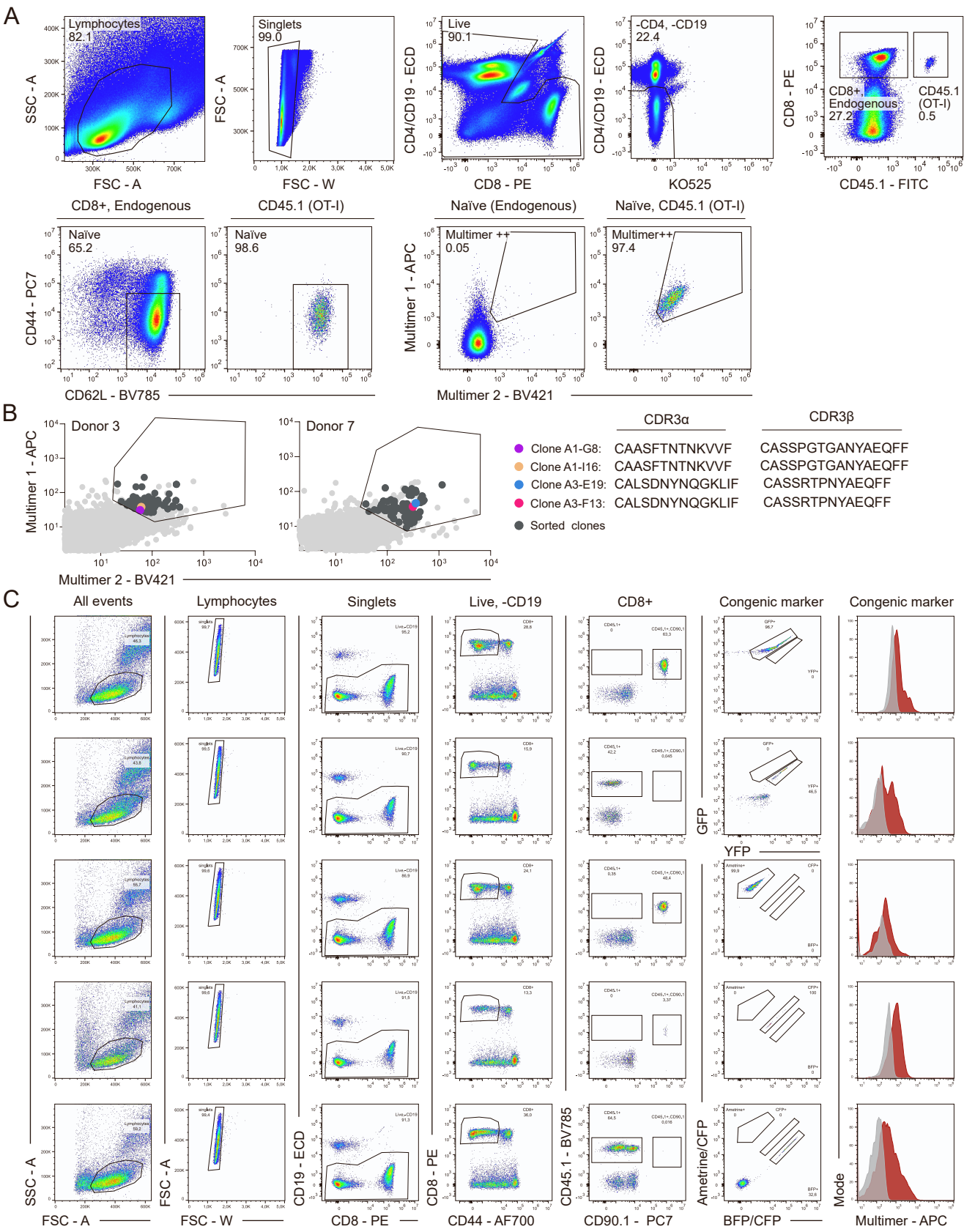


**Figure S2. Sorting strategy and multimer staining of naïve T cells, related to Figure 2.**

(A), Gating for sorting and quantification of SIINFEKL-reactive naïve precursor populations. Numbers indicate percentages. (B), Dot plots depict multimer fluorescence intensities as assessed by index sorting of SIINFEKL-reactive CD8+ T cells. Duplicate clones in the same donors indicate homeostatic proliferation due to similar multimer staining (C), Gating for assessment of multimer staining intensities and expression of color barcodes in retrogenic mice. Numbers indicate percentages.

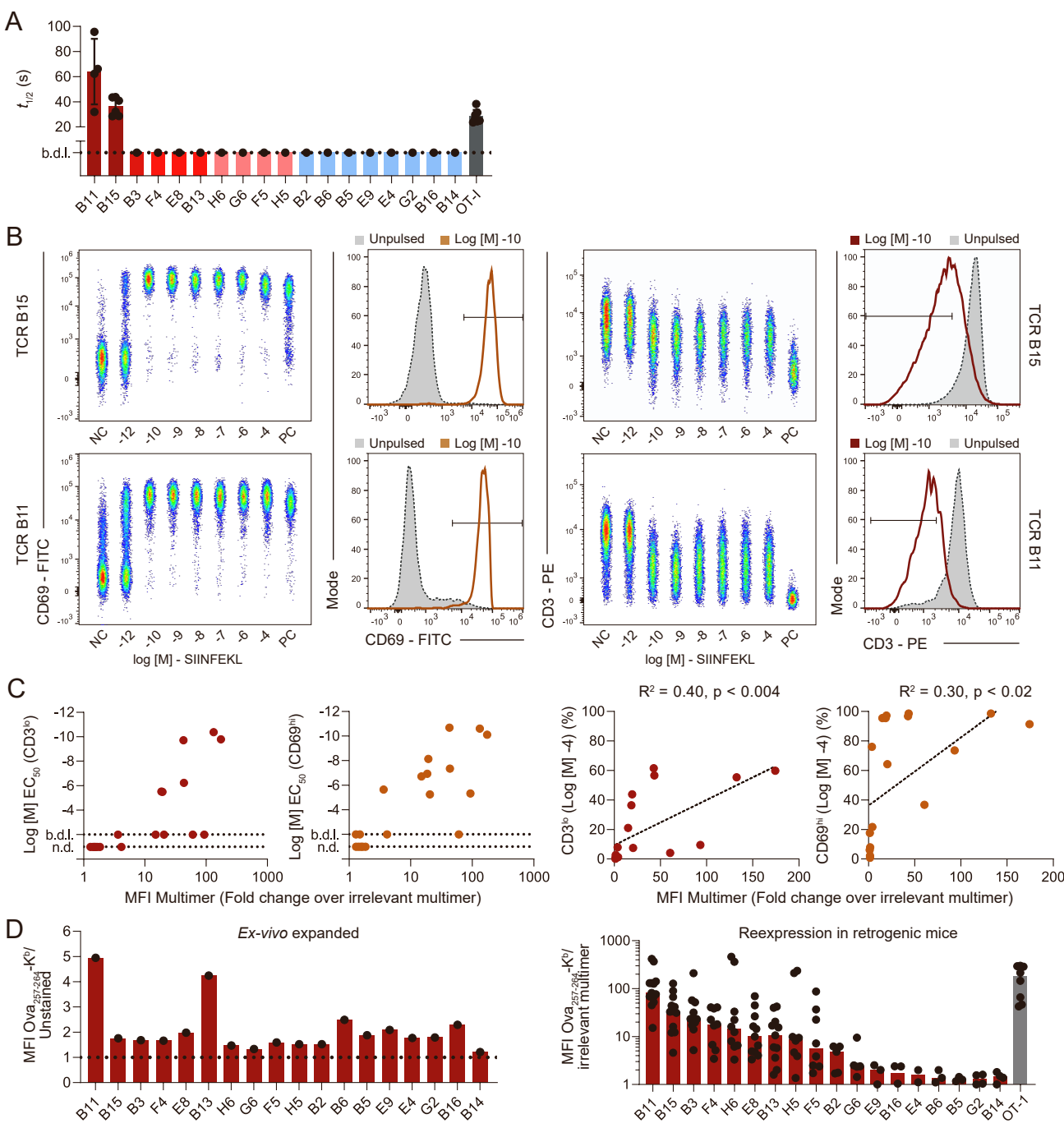
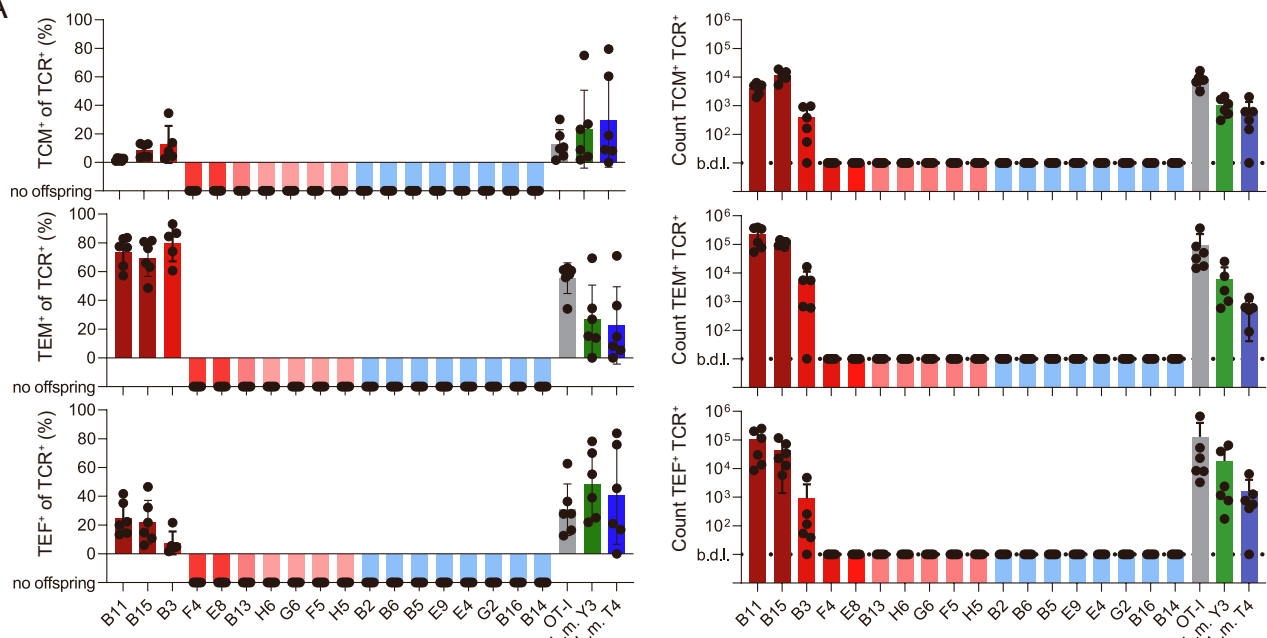


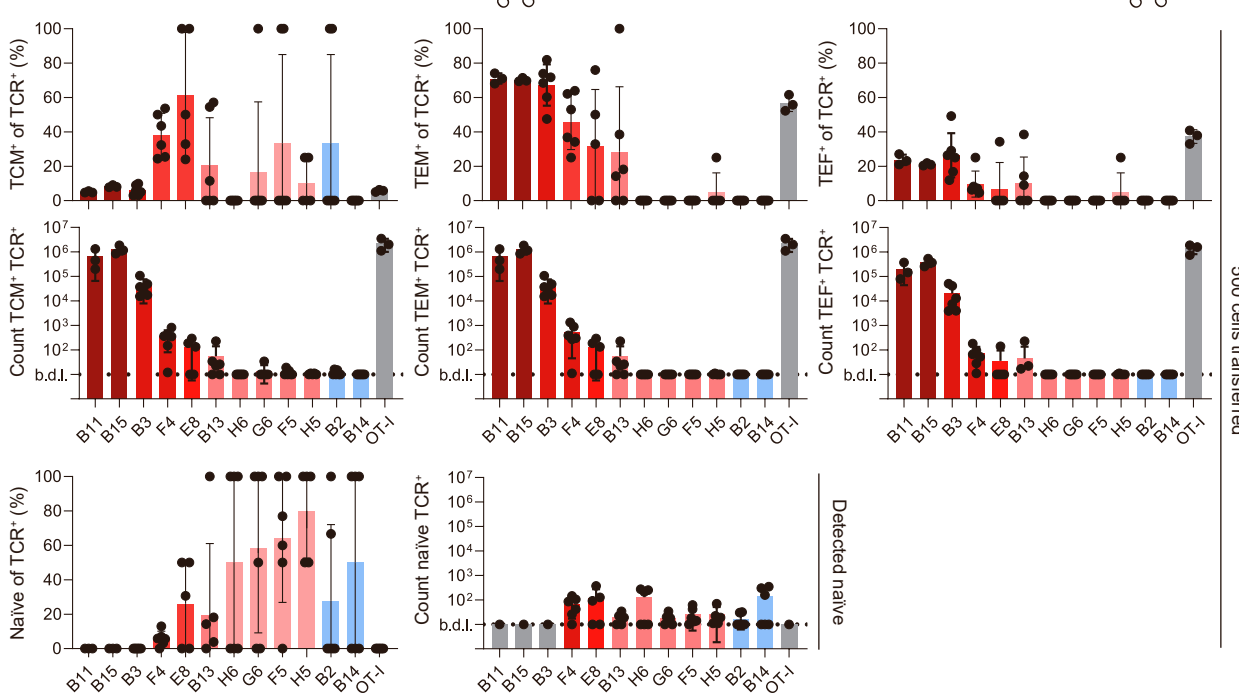
**Figure S3. Gating strategy to assess TCR structural and functional avidity, related to Figure 3.**

(A), Summary of structural TCR avidities ( $t_{1/2}$  s). Each dot represents a replicate for one T cell population from a TCR-retrogenic donor (or transgenic donor for OT-I); bars indicate mean. For each TCR, at least 2 biological replicates of cells from at least two different retrogenic donors were used in independent experiments. (B), Representative FACS data and gating strategy of T cell stimulation via peptide titration shows CD3 downregulation and CD69 upregulation of reexpressed TCRs B11 (n=2) and B15 (n=3). (C), Correlation between Multimer MFI fold change over irrelevant pMHC multimer (M38) from TCR retrogenic mice and functional avidity assessment *in-vitro*, left: correlation with EC<sub>50</sub> (%CD3<sup>lo</sup> and %CD69<sup>hi</sup>), right: correlation with %CD3<sup>lo</sup> and %CD69<sup>hi</sup> at the highest peptide dose (10<sup>-4</sup>M). (D), Multimer restaining of ex-*vivo* expanded CD8<sup>+</sup> T cells (left) and CD8<sup>+</sup> T cells isolated from retrogenic mice (right).

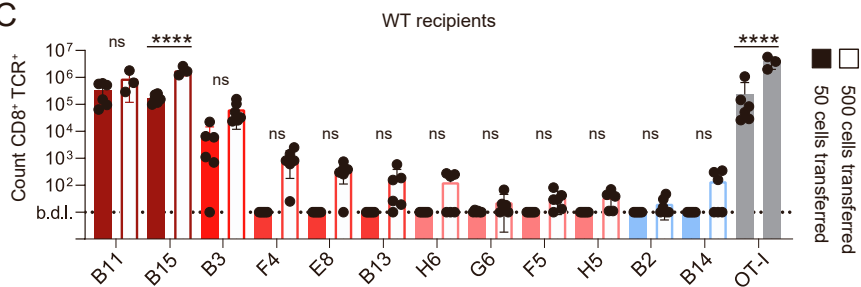
A



B



C



D

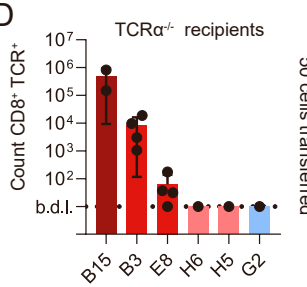


**Figure S4. Differentiation and precursor frequency dependent recruitment of transgenic T cells after transfer and infection, related to Figure 4.**

**Figure S4. Differentiation and precursor frequency dependent recruitment of transgenic T cells after transfer and infection, related to Figure 4.**

(A), Summary of phenotype distribution at day 8 after adoptive transfer of 50 cells of a monoclonal T cell population into WT recipients and L.m.-SIINFEKL infection. Left: Depicted phenotype as percent of recovered retrogenic TCR<sup>+</sup> T cells; right: Abs. numbers of recovered retrogenic TCR<sup>+</sup> T cells with depicted phenotype. Recovered progeny after adoptive transfer of 50 naïve TCR transgenic CD8+ T cells in the spleen. Progeny of 50 naïve OT-I cells on day 8 after L.m.-SIINFEKL (N4, grey), -SIYNFEKL (Y3, green), -SIITFEKL (T4, blue) infection for comparison. In the CD44<sup>hi</sup> compartment, T central memory precursors (TCM), T effector memory and T effector cells are defined as CD62L<sup>hi</sup>, CD27<sup>hi</sup>; CD62L<sup>lo</sup>, CD27<sup>hi</sup> and CD62L<sup>lo</sup>, CD27<sup>lo</sup>, respectively. Naïve T cells are defined as CD44<sup>lo</sup>, CD62L<sup>hi</sup>, n = 6 mice per group per experiment. (B), Data as in (A) but for adoptive transfer of 500 naïve, retrogenic CD8<sup>+</sup> T cells (instead of 50). Data in (A) and (B) are pooled from 19 and 11 independent experiments, respectively, n = 6 mice per group per experiment (except for B11, B15, OT-I, n = 3 mice per group). (C), Recovered progeny at day 8 in the spleen after adoptive transfer of 50 (filled bars) or 500 (empty bars) naïve, retrogenic CD8<sup>+</sup> T cells into WT recipients following L.m.-SIINFEKL infection as shown in Figure 4B-C. Statistical testing was done using a one-way ANOVA followed by Šidák multiple comparisons test. \*\*\*\*p < 0.0001, ns = not significant. (D), Recovered progeny at day 8 in the spleen after adoptive transfer of 50 naïve, retrogenic CD8<sup>+</sup> T cells into Tcra<sup>-/-</sup> recipients following L.m.-SIINFEKL infection; n=4 mice per group except for TCR B15 (n = 2). Bars depict mean.

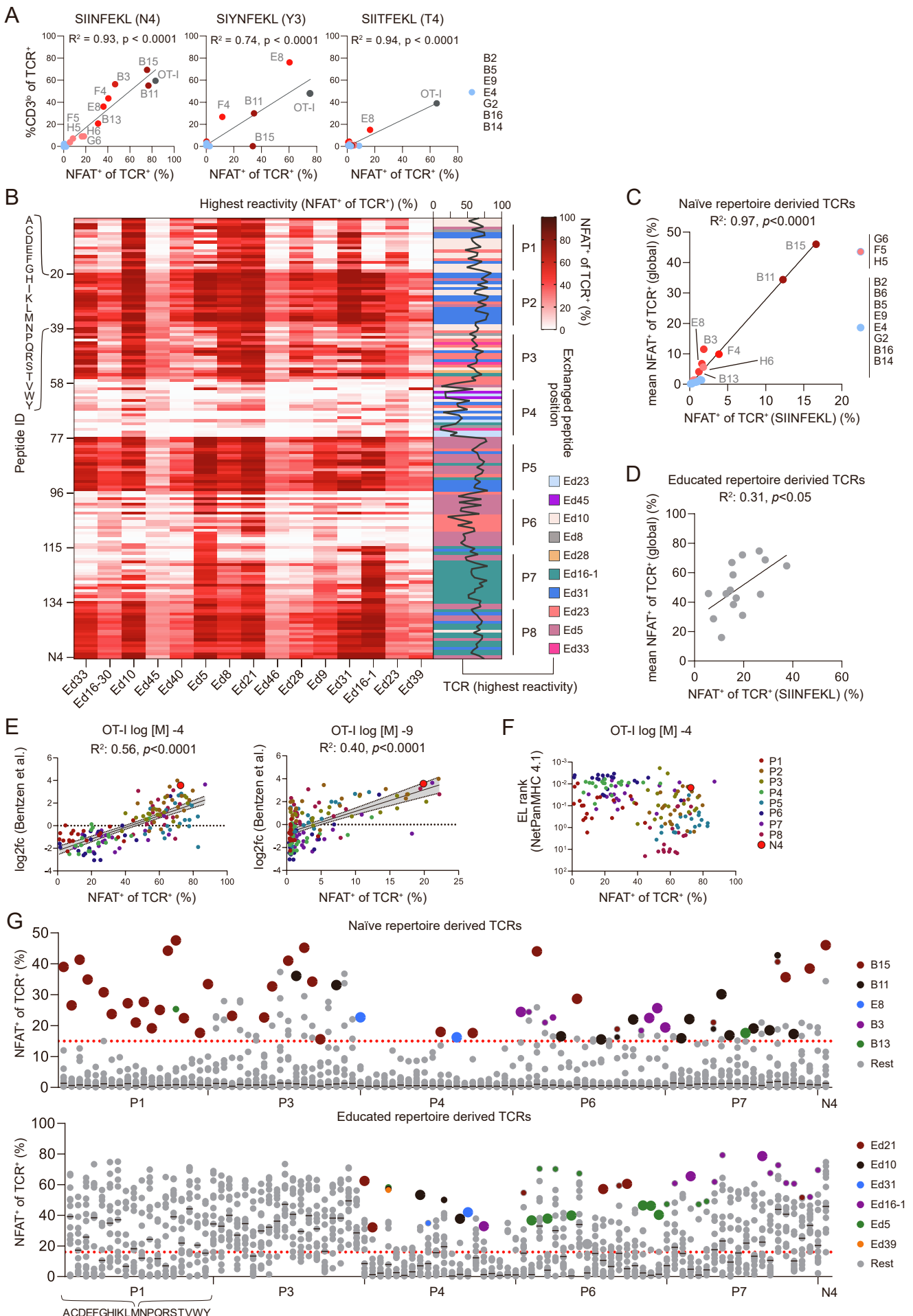


**Figure S5. Correlations between JTPR and primary T cells and activation of educated repertoire derived T cell clones with APLs, related to Figure 5.**

**Figure S5. Correlations between JTTPR and primary T cells and activation of educated repertoire derived T cell clones with APLs, related to Figure 5.**

(A), Correlation between percentage of CD3<sup>lo</sup> TCR transgenic primary murine T cells and percentage of NFAT<sup>+</sup> TCR transgenic JTTPR after antigen-specific stimulation. OT-I interaction for comparison. TCRs are color coded according to their functional avidity towards SIINFEKL from dark red (high avidity, based on CD3 downregulation) to light red (low avidity) to light blue (low avidity, defined through no detectable CD3 downregulation). (B), Peptide stimulation with APL-library of educated repertoire derived TCRs: JTTPR were individually stimulated with 152 APLs of SIINFEKL as well as N4 itself; each amino acid position in the SIINFEKL peptide was exclusively exchanged with every other amino acid, generating 152 unique peptides with single position mutations. APLs are assigned a peptide ID ordered by mutated position (from P1 to P8) and exchanged amino acid (left), N4 depicts unmutated SIINFEKL. Line plot on the right depicts highest measured NFAT expression over the whole repertoire (red line), background coloring shows the respective TCR with highest reactivity for a given APL. (C), Correlation between global NFAT (geometric mean) expression of all measured APLs (y-axis) and SIINFEKL reactivity (x-axis) for naïve repertoire derived TCRs. (D), Data as in (C) but for educated repertoire derived TCRs. (E), Correlations between log fold change of DNA-barcoded bound pMHC molecules as described in Bentzen et al. (2018) and measured NFAT expression after peptide stimulation at different peptide concentrations. (F), Correlations between predicted binding rank (EL rank) of APLs derived from NetMHCpan-4.1 (Reynisson et al., 2020) and measured NFAT expression after peptide stimulation at different peptide concentrations. (G), Peptide stimulation with APL-library as described in (B) highlighting epitopes which are mainly recognized by a single TCR (large dots) or highest reactivities (small dots), reduced to mutated position P1, P3, P4, P6, P7 and SIINFEKL for naïve repertoire (upper) and educated repertoire (lower) derived TCRs. Each dot shows the mean of 2 measurements, red dotted line indicates TCR B3-SIINFEKL interaction. Black lines indicate median. Data in (A), x-Axis display the mean of two technical replicates, data on y-Axis display the mean of independent experiments ( $n = 2$  to 4). Data in (B) are pooled from 15 independent experiments, NFAT expression is displayed as the mean of two technical replicates. For data in (A), (C), (D) and (E) a regression line was fitted with a linear regression model, for data in (E) including 95% confidence intervals (gray).

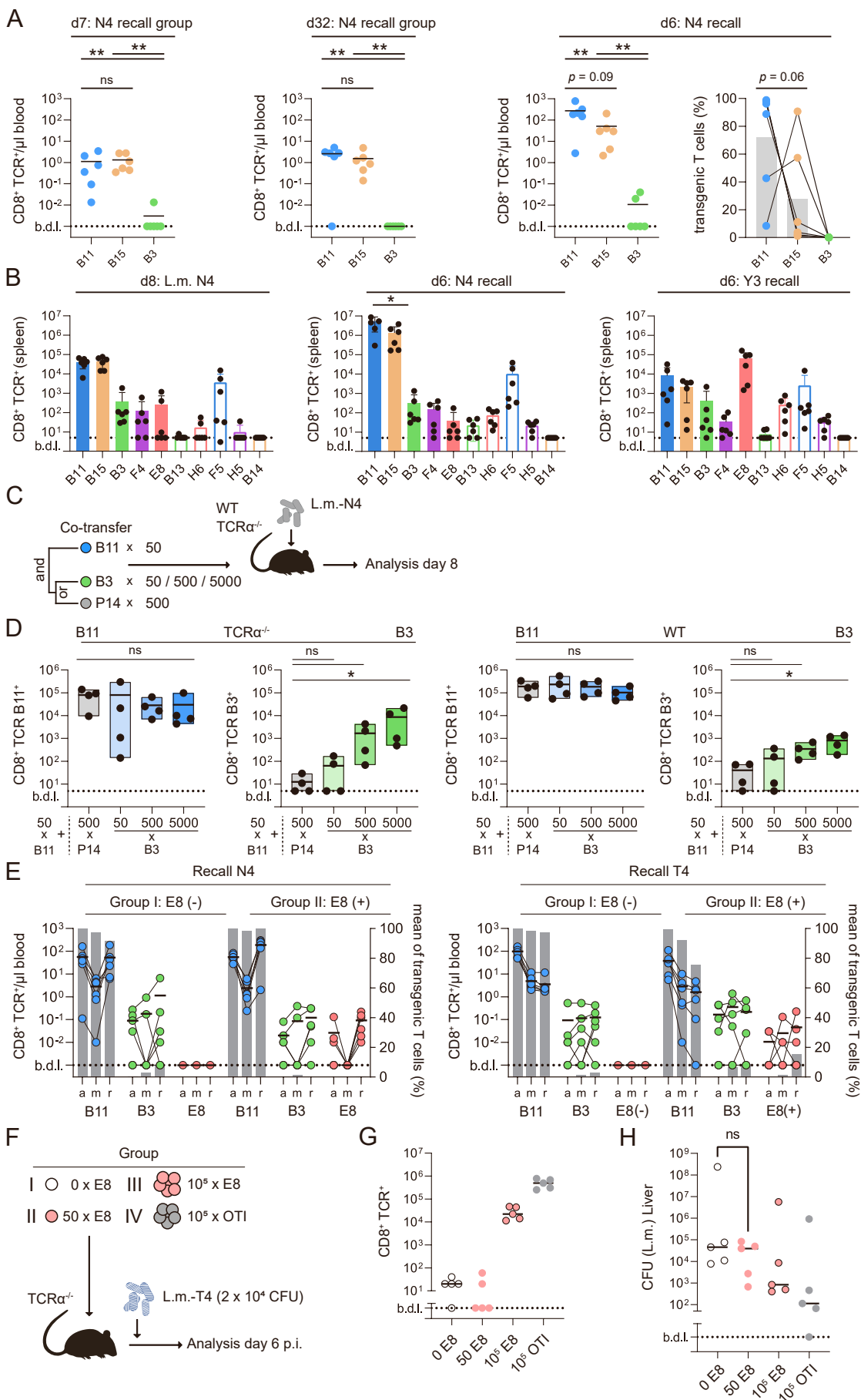


**Figure S6. Recovered transgenic T cells after polyclonal transfer and infection and interclonal competition in  $Tcr\alpha^{-/-}$  recipients, related to Figure 6.**

**Figure S6. Recovered transgenic T cells after polyclonal transfer and infection and interclonal competition in  $Tcra^{-/-}$  recipients, related to Figure 6.**

(A), Scatter plots depict recovered T cell clones in blood after transfer of 10 different TCRs of recipients which received a secondary L.m.-N4 infection as in Figure 6A, 6E. From left to right: recovered clones for TCR B11, B15 and B3 (others not shown) at day 7, 32 and day 6 post secondary infection, lines depict mean; percentage of transgenic T cells at day 6 post secondary infection, bars depict mean. Statistical testing by Mann–Whitney test. \*\* $p < 0.001$ . (B), Recovered T cell clones from spleen at day 8 post primary infection, day 6 post secondary infection with L.m.-N4, day 6 post-secondary infection with L.m.-Y3. Bars depict mean ( $n = 6$  per group). (C), Schematic of experimental setup: Co-transfer of 50 B11 and increasing numbers of B3 or control P14 cells (LCMV gp<sub>33-41</sub>) into wild type or  $Tcra^{-/-}$  recipients, followed by infection with  $5 \times 10^3$  CFUs of L.m.-N4. (D), Box plots: Recovered T cell clones from B11 (blue) and B3 (green) at day 8 pi. in spleen ( $n=4$  per group); left:  $Tcra^{-/-}$  recipients, right: WT recipients. Gray box plots depict co-transfer of 50 B11 or 50 B3 cells against 500 P14 cells, respectively. Box plots depict mean and range. Statistical testing by Kruskal-Wallis test followed by Dunn's multiple comparison test. \* $p < 0.05$ . (E), Scatter plots depict recovered T cell clones as in Figure 6F in blood at three different time points; a: acute (d7 p.i.), m: memory phase (d40 p.i.), r: recall (d6 p. secondary infection); dots show TCR transgenic T cells per  $\mu$ l blood (left y-axis), bars show mean fraction of recovered T cell clones (right y-axis); left panel:  $Tcra^{-/-}$  recipients rechallenged with L.m.-N4; right panel:  $Tcra^{-/-}$  recipients rechallenged with L.m.-T4 ( $n = 6$  per group). (F), Schematic of experimental setup: Transfer of 0, 50,  $10^5$  naïve E8 or  $10^5$  naïve OT-I cells into  $Tcra^{-/-}$  recipients ( $n = 5$  per group), followed by infection with  $2 \times 10^4$  CFUs of L.m.-T4. (G), Scatter plots depict recovered T cell clones on day 6 p.i in spleen. (H), CFUs of L.m. isolated from liver of recipient mice after infection. Ns, not significant, B.d.l., below detection limit, lines depict median, statistical testing by Mann–Whitney test.